



Multi-scale variations in invertebrate and fish megafauna in the mid-eastern Clarion Clipperton Zone

Erik Simon-Lledó^{a,*}, Christina Pomee^b, Akesa Ahokava^b, Jeffrey C. Drazen^c, Astrid B. Leitner^d, Adrian Flynn^e, John Parianos^f, Daniel O.B. Jones^a

^a National Oceanography Centre, Southampton, United Kingdom

^b Tonga Offshore Mining Ltd., Nuku'alofa, Tonga

^c University of Hawaii Manoa, Honolulu, USA

^d Monterey Bay Aquarium Research Institute, Moss Landing, USA

^e Fathom Pacific Pty Ltd., Melbourne, VIC, Australia

^f Nautilus Minerals, Brisbane, QLD, Australia

ARTICLE INFO

Keywords:

Biodiversity
Abyssal hills
Polymetallic nodules
Deep-sea mining
Biogeography

ABSTRACT

The abyssal seafloor of the Clarion Clipperton Zone (CCZ) in the central Pacific has the largest known deposits of polymetallic nodules and associated benthic faunal communities with high biodiversity. The environmental factors that structure these communities, both at regional and local scales, are not well understood. In this study, seabed image surveys were used to assess distribution patterns in invertebrate and fish megafauna (> 1 cm) at multiple scales in relation to key environmental factors: food supply to the seabed varying at the regional scale (hundreds of km), seabed geomorphological variations varying at the broad local scale (tens of km), and seabed nodule cover varying at the fine local scale (tens of meters). We found significant differences in megafaunal density and community composition between all study areas. Variations in faunal density did not appear to match with regional productivity gradients, although faunal density generally decreased with increasing water depth (from E to W). In contrast, geomorphology and particularly nodule cover appeared to exert strong control on local faunal abundance and community composition, but not in species richness. Local variations in faunal density and beta-diversity, particularly those driven by nodule presence (within study areas), were of comparable magnitude to those observed at a regional level (between study areas). However, regional comparisons of megabenthic assemblages showed clear shifts in dominance between taxonomic groups (perceivable even at Phylum levels) across the mid-eastern CCZ seabed, suggesting a higher regional heterogeneity than was previously thought.

1. Introduction

Global economic interest in deep-sea mining has grown since the discovery of extensive polymetallic nodule fields in the equatorial Pacific during the HMS *Challenger* expedition (Murray and Renard, 1891). Abyssal plain and hill environments of the Clarion Clipperton Zone (CCZ) in the central eastern Pacific harbour the largest known deposits of polymetallic nodules, rich in manganese, copper, nickel, and cobalt (Hein et al., 2020). Nodule fields constitute an unusual mosaic habitat in the deep sea (Simon-Lledó et al., 2019b). The hard substratum provided by nodules combined with the background soft sediment acts to increase habitat complexity (Simon-Lledó et al., 2019b), which is thought to promote the occurrence of some of the most biologically diverse seafloor assemblages in the abyss (Amon et al., 2016;

Christodoulou et al., 2020; Gooday et al., 2017; Janssen et al., 2015). However, at present, the ecology of these remote habitats is poorly understood, little is known of the environmental factors that drive biodiversity nor the scales at which these operate, and the available biogeographical information is sparse, especially towards the mid-western CCZ.

Abyssal benthic communities are strongly modulated by the flux of particulate organic carbon (i.e. food) sinking through the water column from the euphotic zone (Johnson et al., 2007; Smith et al., 2008). At the CCZ seafloor, where depositional fluxes are generally low (e.g. 1–2 mg C_{org} m⁻² d⁻¹; Lutz et al., 2007; Volz et al., 2018), communities typically exhibit low faunal abundance but a surprisingly high biodiversity (e.g. Glover et al., 2002; Janssen et al., 2015). Regionally, the closer proximity of the southern areas of the CCZ to the equatorial Pacific

* Corresponding author.

E-mail address: erimon@noc.ac.uk (E. Simon-Lledó).

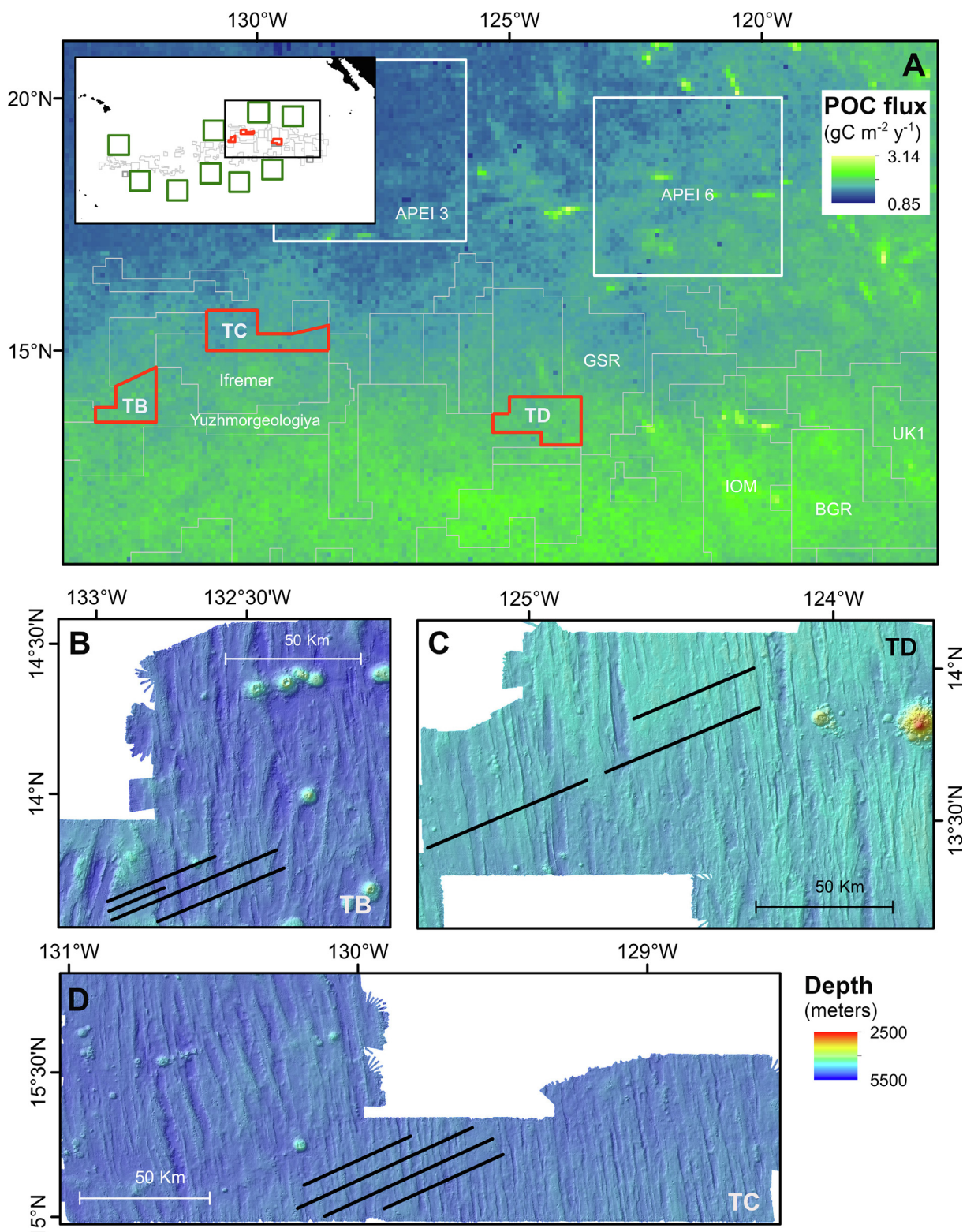


Fig. 1. Survey locations within the mid-eastern Clarion Clipperton Zone (CCZ). (A) Nutrient flux from surface to the seafloor across the mid-eastern CCZ, as reported by Lutz et al. (2007). Red polygons represent the three TOML exploration areas (TB, TC, and TD) target of the present study. Grey polygons represent other exploration licensed areas. White polygons represent Areas of Particular Environmental Interest (APEIs). Image-based megafauna studies have been conducted in all areas with name displayed (see Discussion). A map is inset depicting the location of this sector (grey rectangle) within the CCZ. (B–D) Bathymetric survey charts of the three study areas with detail of image transect locations (dark lines). (B) TOML Area B. (C) TOML Area D. (D) TOML Area C. (For interpretation of the references to colour in this figure legend, the reader is referred to the web version of this article.)

high-productivity zone (e.g. Pennington et al., 2006) has been linked with enhanced invertebrate density and species richness in the benthic communities found beneath (Błażewicz et al., 2019; Glover et al., 2002; Vanreusel et al., 2016; Veillette et al., 2007; Wilson, 2017). Differences in density, diversity and/or body size correspond with productivity gradients observed among the CCZ region in dominant smaller-sized invertebrate groups, such as Polychaeta (Bonifácio et al., 2020; Wilson, 2017), Tanaidacea (Błażewicz et al., 2019; Wilson, 2017), and Nematoda (Hauquier et al., 2019; Lamshead et al., 2003; Macheriotou et al., 2020), although Isopoda show more variable biogeographical patterns (Brix et al., 2019; Wilson, 2017). Fewer assessments have been conducted at a regional scale (e.g. hundreds of km) in megafauna groups (e.g. invertebrates and fish > 1 cm). Vanreusel et al., (2016) depicted the substantially lower benthic megafauna density in the Area of Particular Environmental Interest 3 (APEI3) compared to the more productive southern areas in the eastern CCZ, in both mobile (e.g. Holothuroidea) and sessile taxa (e.g. Alcyonacea soft corals). In contrast, a recent study conducted across the western border of the CCZ (Kiribati EEZ) failed to find any correspondence between megafaunal community features and nutrient flux gradients (Simon-Lledó et al., 2019d). Further assessment of the correspondence between nutrient flux variations and the megafauna -measurable across large seabed areas using imagery data- can be important to better define biogeographical provinces in the CCZ, particularly if coupled with other environmental factors operating at more local scales.

Environmental drivers operating at a local scale within the CCZ seabed, e.g. within exploration license areas or APEIs, have the capacity to drive changes in the benthic community, particularly in megafauna assemblages (Simon-Lledó et al., 2019a,b). At a broader scale, e.g. tens of km, variations in megafaunal abundance and composition have been encountered between adjacent plains, hills and troughs in invertebrate (Simon-Lledó et al., 2019a) and bait-attending (Leitner et al., 2017) assemblages, comparable to variations in other abyssal hill and plain environments in the north Atlantic (Durden et al., 2015; Stefanoudis et al., 2016). At the finer scale, of tens of meters, variations in faunal abundance and community structure have been described between seabed areas with different nodule availability for megafauna (Amon et al., 2016; Simon-Lledó et al., 2019b), macrofauna (Chuar et al., 2020; Mullineaux, 1987), meiofauna (Miljutina et al., 2010; Singh et al., 2016), and foraminifera (Kamenskaya et al., 2013; Simon-Lledó et al., 2019b). These changes are thought to be related to the increased habitat heterogeneity associated with the presence of nodules, as nodule-dwelling taxa can represent 60–70% of the total numerical abundance of fauna present in nodule fields (Amon et al., 2016; Simon-Lledó et al., 2019b). Broad-scale geomorphological variations can regulate bottom water speeds and particle deposition rates in the CCZ (Skornyakova and Murdmaa, 1992), which are factors that are presumed to modulate nodule growth (Mewes et al., 2014). However, there is no simple relationship between nodule cover and seafloor morphology (Peukert et al., 2018) and hence the effect of each factor on benthic fauna is best assessed independently.

Sixteen nodule mining exploration contract areas have been so far granted in the CCZ by the International Seabed Authority (ISA, 2020), the institution responsible for the management of these resources along with the conservation and protection of the marine environment (Lodge et al., 2014). The ISA requires contractors to document the biota in their license area (Durden et al., 2018; Jones et al., 2019), as the effective management of potential exploitation activities will rely on such baseline information. In 2011, Tonga Offshore Mining Limited (TOML) was granted 6 exploration areas (TOML A, B, C, D, E, and F) by the ISA (NM, 2016) that are spread throughout a wide longitudinal range from west to east across the CCZ. Two expeditions to these sites were conducted by TOML in 2013 and 2015 to map the seafloor and to collect geotechnical and environmental baseline data (NM, 2016). During these expeditions, a vast area of seafloor (~75,000 m²) was imaged at high photographic resolution across three of the exploration-licensed

sites (i.e. TOML B, C, and D; Fig. 1) in the mid-eastern CCZ.

In this paper we present an analysis of megafaunal distributions based on seabed imagery collected in three of TOMLs contract areas (B, C and D) in the CCZ. We explore variations in megabenthic community structure at the large (regional) scale between sites and couple this with independent assessments for each contract area performed at the finer (local) scale, to investigate how variations in the presumed food supply regime, seabed geomorphology, and nodule cover may affect the distribution of megafauna in the mid-eastern CCZ abyss. We discuss these results in the context of similar studies previously conducted in the eastern CCZ to draw preliminary biogeographical patterns along this region.

2. Methods

2.1. Study areas

Data used in this study were acquired during the RV *Mt Mitchell* (2013) and the RV *Yuzhmorgeologiya* (2015) expeditions (NM, 2016) to the mid-eastern CCZ TOML exploration areas B, C, and D, between 13 and 15° N and 123 to 133° W, in the Pacific Ocean (Fig. 1). Four target areas of about 2000 km² were chosen across TOML areas B, C and D: respectively B1, C1, D1 & D2 (NM, 2016) and hereafter referred to as study areas TB (TOML B1), TC (TOML C1), and TD (TOML D1 + D2). Areas TB and TC are ~350 km apart at a similar water depth (~5000 m, Table 1), while Area TD area is ~500 m shallower, ~550 and ~850 km away from areas TC and TB respectively. As is commonplace in central areas of the CCZ (Olive et al., 2015), the seafloor landscape of the three study areas is comprised of a succession of parallel abyssal hills and

Table 1

Survey details and environmental features of each study area. **Box-core surveys:** mean abundance and proportions of different nodule type- and size-classes. **Image surveys (this study):** water depth (mean value and range) across the images collected; mean seabed nodule cover across the images collected; total abundance and number of megafauna morphotypes detected in images. **Other data:** POC flux to the seabed (mean value and range within the surveyed area).

	TOML B	TOML C	TOML D
Box-core surveys^{*1}			
Nodule abundance (wet kg m ⁻²)	9.93 ± 8.25	7.41 ± 5.54	12.71 ± 7.53
Nodule type			
– Smooth (S)	14%	27%	9%
– Smooth-rough (SR)	62%	73%	74%
– Rough (R)	24%	0%	16%
Nodule size (max. diameter)			
– Small (< 2 cm)	32%	20%	14%
– Medium (2–5 cm)	29%	60%	31%
– Large (> 5 cm)	39%	20%	56%
Image surveys			
Images collected (usable)	6,932	8,124	5,611
Seabed area imaged (m ²)	24,955	29,246	20,200
Water depth (m)	4917 (4418–5175)	4926 (4817–5065)	4557 (4345–4750)
Mean nodule cover (%)	33.7 ± 24.0	37.3 ± 26.8	13.2 ± 10.6
Individuals (invertebrates)	3567	3377	8902
Total taxa (invertebrates)	168	145	189
Individuals (fish)	46	83	76
Total taxa (fish)	11	14	10
Other data (from lit.)			
POC flux (g C m ⁻² y ⁻¹) ^{*2}	1.58 (1.53–1.61)	1.53 (1.50–1.56)	1.58 (1.51–1.62)

^{*1} Obtained from NM NI 43-101 Technical report, 2016.

^{*2} Derived from Lutz et al. (2007).

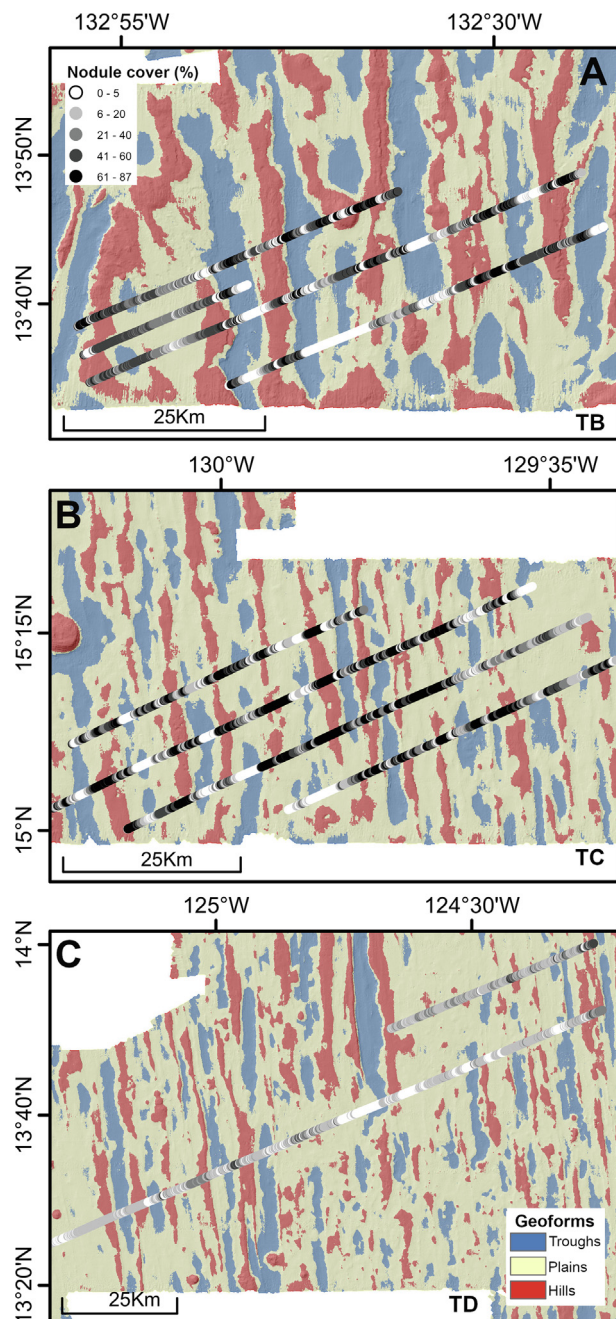


Fig. 2. Variations in seabed geomorphology and nodule-cover mapped within each TOML study area. Lines represent image survey locations. (A) Area TB. (B) Area TC. (C) Area TD.

shallow troughs oriented north–south between dispersed flatter areas (Fig. 1), with a depth range (e.g. hilltops to trough bottom) between 300 and 500 m (see Fig. A1).

The seafloor of the three study areas is composed of unconsolidated sediment and polymetallic nodules with notable differences in shape (e.g. smooth, S; rough, R; smooth-rough, SR) and size (maximum diameter: small < 2 cm; medium 2–5 cm; large > 5 cm). The shape of nodules is thought to be controlled by the formation mechanism, with the smooth nodules being formed predominantly by hydrogenetic growth, the rough nodules by diagenetic growth and the smooth-rough type being formed at the sediment-water interface with hydrogenetic growth on top and diagenetic growth on the underside (NM, 2016). Area TC has very few large nodules with medium sizes and SR shapes dominating in box-core samples (NM, 2016; Table 1). Nodules in areas

TB and TD are mostly of SR type and exhibit a wider range of sizes, although the proportion between nodule size categories was more even in Area TB than in TD, as substantially larger nodules were found in box-core samples collected in Area TD (NM, 2016; Table 1). Consequently, although nodule cover (% seabed surface, in images) was generally lower in Area TD than in areas TB and TC (see Section 2.2 and Fig. 2), the mean nodule abundance (wet kg, in box-core samples) was higher within Area TD (NM, 2016; Table 1). Additionally, two types of ferromanganese crusts were observed across the three study areas, all commonly found at the CCZ (e.g. Radziejewska, 2014). Massive crust 5–10 cm thick and typically found in blocks of 20–50 cm diameter (and occasionally as pavement); while crustal-nodules are small to medium sized (diameter < 20 cm) discrete fragments of ferro-manganese that can grade into nodules (NM, 2016). In total, crusts were found in ~0.6% of areas surveyed, with crustal nodules more common (~0.5%) and massive crusts being present only ~0.1% of the seabed mapped (NM, 2016). Zeolite sheets, a third crust-like material that is very rarely encountered (Venkatarathnam and Biscaye, 1973), were identified in just a few locations in Area TB, and in one location in Area TD (NM, 2016).

2.2. Environmental assessment

2.2.1. Bathymetric mapping and landscape characterization

Bathymetric data were used to map different geomorphological units (i.e. geoforms) within each study area. Multibeam data were collected with the shipboard Kongsberg EM120 MBES system (191 beams) and processed using CARIS HIPS and SIPS software (TeledyneCARIS; v8.0). The resultant digital elevation model (60 m horizontal resolution) was used to calculate a broad bathymetric position index (BPI; Weiss, 2001) using the Benthic Terrain Modeler tool (Wright et al., 2012) implemented in ArcGIS v10.2 (ESRI, 2012). BPI was calculated using an inner radius of 2.5 km and an outer radius of 5 km to match the horst and graben structure that typically shapes the central areas of the CCZ (usual wavelength: 10 km W-E; e.g. Olive et al., 2015). After visual inspection of the resultant datasets, classification thresholds were set to map hills ($BPI > 50$), plains ($BPI: -50$ to 50), and troughs ($BPI < -50$) within each study area (Fig. 2; Fig S1). Data were projected in Universal Transverse Mercator projection - Zones 8 N (Area TB), 9 N (Area TC) and 10 N (Area TD) - using the World Geodetic System 1984 datum.

2.2.2. Image data collection

Seafloor images were collected using a digital camera (Canon D60; 3456 × 2304 pixels) mounted on the towed camera system Neptune, developed by the Russian marine institute JSC Yuzhmorgeologiya (NM, 2016). The Neptune system was towed at a speed of 0.1–0.2 m s⁻¹ and pictures were taken at an altimeter-triggered altitude of 3.5 m above the seafloor, with an interval of at least every 30 s to avoid overlap between frames. At the target altitude, individual photographs imaged 3.6 m² of seabed. A total of 11 image transects were collected using the Neptune system across the three study areas (Figs. 1 and 2). Four transects were surveyed in Area TB (total seabed area: 24,955 m²), four in Area TC (total seabed area: 29,246 m²), and 3 in Area TD (total seabed area: 20,199 m²). The full resultant dataset comprised a total of 20,667 non-overlapping images, representing a total seafloor area of 74,401 m² (Table 1).

2.2.3. Nodule cover assessment

Nodule cover (%) of the seabed was quantified in each image using a custom MATLAB (The Math Works Inc.) routine based on colour contrast. This routine performed a binary classification of each image pixel, e.g. sediment (bright coloured) or nodule (dark coloured) substrate, based on visually determined RGB thresholds, to then estimate the approximate seafloor exposed area composed by nodules or rocks in each image.

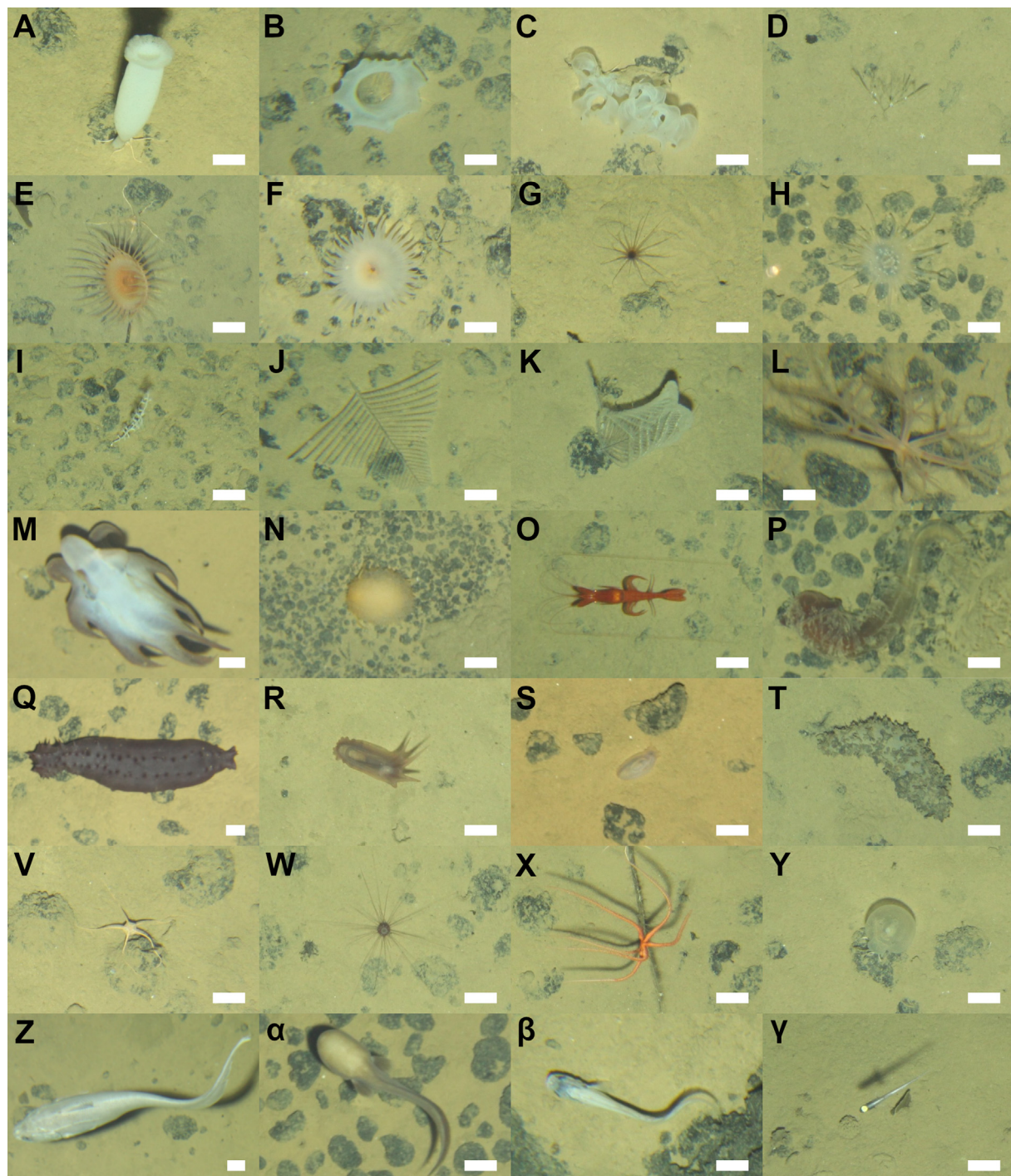


Fig. 3. Examples of megafauna photographed during towed-camera surveys. Scale bar = 5 cm. (A–Z) Invertebrates. (A) Euplectellidae mtp-5. (B) *Holascus euonyx* sp. inc. (C) Porifera mtp-77. (D) Bryozoa mtp-5. (E) Actiniaria mtp-9. (F) Actiniaria mtp-2. (G) Ceriantharia mtp-1. (H) Corallimorpharia mtp-3. (I) *Bathygorgia* sp. mtp-5. (J) *Schizopathes* sp. mtp-1. (K) *Abyssopathes lyra* sp. inc. (L) *Umbellula* sp. mtp-3. (M) *Grimpoteuthis* sp. mtp-1. (N) Nudibranchia mtp-1. (O) *Cerataspis monstrosus* sp. inc. (P) Torquatoridae mtp-5. (Q) *Psychronautes hanseni* sp. inc. (R) *Amperima* sp. mtp-3. (S) *Ellipinion* sp. mtp-1. (T) *Pseudostichopus* sp. mtp-2. (V) *Ophiospalma glabrum* sp. inc. (W) *Aspidodiadema* sp. mtp-1. (X) *Freyastera* sp. mtp-2. (Y) *Phlebobranchia* mtp-16. (Z–γ) Fishes. (Z) *Coryphaenoides* sp. (α) *Typhlonus nasus*. (β) *Leucicorus* sp. (γ) *Ipnops meadi* sp. inc.

2.3. Biological assessment

Images were annotated using a two-step approach. Metazoan megafauna specimens (> 1 cm) were first detected and then identified to the lowest taxonomic hierarchy possible (morphotype [mtp]: typically Genus or Family level) using BIIGLE 2.0 (Langenkämper et al., 2017). To ensure consistency in specimen identification, abyssal-Pacific standardized megafauna catalogues (invertebrates and fish, some

examples shown in Fig. 3) were compiled from previous studies in the basin and by reference to existing literature (Amon et al., 2017; Dahlgren et al., 2016; Drazen et al., 2019; Kersken et al., 2019; Molodtsova and Opresko, 2017; Simon-Lledó et al., 2019b, 2019c, 2019d). The likely feeding behaviour of each morphotype was inferred from similar organisms described in the literature. Although xenophyophores were the most abundant specimens on the seabed (up to 15–20 tests per image) these were not included in this study as it is not

possible to determine whether foraminiferal tests are alive in images (Hughes and Gooday, 2004). Similarly, invertebrates living in a shell or tube (e.g. most polychaete and gastropod taxa) were also excluded from the analyses. Specimen counts in each image are provided in the Supplementary material: Appendix A.

2.3.1. Data analysis

Patterns in diversity and distribution of fauna were investigated at different scales: i) regionally, between geographically distant study areas (hundreds of km: areas TB, TC, and TD), ii) locally, at a broad-scale, between different geoform types of each study area (tens of km: Troughs, Plains, and Hills), and iii) locally, at a fine-scale, along the gradient of seabed nodule-cover of each study area (tens of meters; nodule cover levels L1 to L5). A different analytical approach was applied to conduct each of these three assessments. A stratified random sampling design (Andrew and Mapstone, 1987) was used for the regional assessment, with true replication across study areas. However, the information needed to assess local patterns was only available from photographic/terrain analysis (nodule abundances) and mapping work both done after sampling. Thus, to control the impact of the physical sample size on the estimation of ecological parameters, we chose to apply a modified form of bootstrapping (Davison and Hinkley, 1997; Manly, 2007) to explore variations between different strata in the local assessments. Resampling techniques provide robust estimates of variability and confidence intervals of sample parameters (Crowley, 1992; Rodgers, 1999), and are particularly well suited to analyse data derived from survey designs that lack true sample replication (see e.g. Simon-Lledó et al., 2019b, 2019d). Note though that given the relatively low total number of fish megafauna observations (208 specimens), and that some deep-sea fish groups can exhibit avoidance behaviour to towed camera systems (e.g. McIntyre et al., 2015), fish distribution data were analysed separately from invertebrates and using a more simplistic approach (i.e. no sample replication). Total fish observations were collated for each of the strata of interest targeted in the study (regional study areas, local geoforms, and local nodule cover levels) relative to the total seabed area sampled and results are consequently presented with no associated error margins. Data processing and analyses were implemented in R (R Core Team, 2017) using functions provided in the ‘vegan’ package (Oksanen et al., 2018), unless specified differently.

2.3.1.1. Regional assessment. Image data (faunal records in images) were pooled for each separate study area ($n = 3$: areas TB, TC, and TD) to investigate variations in faunal characteristics at the regional scale. Following recommendations for optimal image-based megafauna sampling at the CCZ (Ardron et al., 2019; Simon-Lledó et al., 2019a), image data from each study area were randomly sampled without replacement to generate replicate samples with a fixed minimum size of 500 individuals (range: 500–503 ind.). This process yielded 7 replicate samples for Area TB, 6 for Area TC, and 17 for Area TD, each encompassing a different seabed area coverage (range: 1098–4424 m²). A set of ecological parameters were calculated for each replicate sample: numerical density (ind. m⁻²) and Hill’s diversity numbers of order 0 and 2 (Jost, 2006), respectively morphotype richness (S_I) and the inverse form of Simpson’s index (1/D). Morphotype density (S_A) was also calculated following a controlled seabed-area approach: images were randomly resampled with replacement to generate bootstrap-like samples with a fixed size of 1000 m² (278 images). Mean values of these parameters were calculated from each bootstrap-like sample set, together with corresponding 95% confidence intervals based on the simple percentile method (Davison and Hinkley, 1997). We report statistical assessments of variations in ecological parameters between study areas by comparisons of the 95% confidence intervals, i.e., the upper limit of a given estimate must be lower than the lower limits of the estimate that is compared to. Such cases are significant at $p < 0.05$, though the true (undetermined) p-value will, necessarily, be considerably lower. Variations in community composition were assessed on a set of 10 randomly selected bootstrap-like samples for each geoform type (in each study area), based on β_{BC} calculated from square-root transformed faunal abundance, and then visualised using MDS ordination.

2.3.1.2. Local assessments. Image data were ordered by estimated nodule cover within each study area to investigate variations in faunal characteristics along the nodule cover gradient. Image data were then divided into 5 subsets at nodule-cover breakpoints chosen to yield approximately equal numbers of megafaunal observations in each subset (levels L1 to L5, each representing a different nodule-cover range in each study area). This survey design resulted in 15 subsets (five for each study area) with

histograms and QQ plots. Models were fitted with Gaussian errors (Freund and Littell, 1981). Where significant differences were detected in global tests, multiple comparisons tests were conducted between individual study areas using the ‘multcomp’ package (Hothorn et al., 2017), p-value adjustments for multiplicity were made using the ‘mvt’ single-step procedure (Hasler and Hothorn Ludwig, 2011). The effect size measure η^2 (eta-squared, Levine and Hullett, 2002) was also calculated to assess magnitude of the variations encountered, using the ‘sjstats’ package (Lüdecke, 2018).

Variations in community composition between study areas were assessed following an abundance-based multivariate approach. Dissimilarity in faunal composition between all pairs of (c. 500 ind.) replicate samples was calculated using the Bray-Curtis dissimilarity measure, i.e. beta-diversity (β_{BC}), based on square-root transformed faunal abundance. Non-metric multidimensional scaling (MDS) ordination was conducted, to visualize the rate of dissimilarity between all pairs of replicate samples. A one-way permutational MANOVA (PERMANOVA) analysis (Anderson, 2001) with follow-up pairwise tests was used to test for statistically significant variations in assemblage composition between study areas.

Taxon accumulation curves were calculated to assess the representability of the sampling conducted, following Colwell et al. (2012), by random resampling of pooled image data for each study area 100 times without replacement forming increasingly larger sampling units, using EstimateS v.9.1 software (Colwell, 2013). Additionally, rank-abundance and taxa intersection plots between sites were also generated (Supplementary material: Appendix A).

2.3.1.2.1. Local assessments

2.3.1.2.1. Geomorphological strata (broad-scale). Image data were split for each geoform (i.e. Troughs, Plains and Hills) within each separate study area to investigate variations in faunal characteristics between geomorphological units. This survey design resulted in 9 subsets (three for each study area) with markedly uneven sample sizes, e.g. specimen counts in each subset ranged between 765 and 5469 individuals (see Table A2). To implement the bootstrap, each image data subset was randomly resampled with replacement until a minimum of 500 individuals were encountered (range: 500–502 ind.), and that process was repeated 1000 times for each geoform type. The same set of ecological parameters assessed at the regional scale were calculated for each bootstrap-like sample: numerical density (ind. m⁻²); morphotype richness (S_I), and the inverse form of Simpson’s index (1/D). Morphotype density (S_A) was also calculated following a controlled seabed-area approach: images were randomly resampled with replacement to generate bootstrap-like samples with a fixed size of 1000 m² (278 images). Mean values of these parameters were calculated from each bootstrap-like sample set, together with corresponding 95% confidence intervals based on the simple percentile method (Davison and Hinkley, 1997). We report statistical assessments of variations in ecological parameters between study areas by comparisons of the 95% confidence intervals, i.e., the upper limit of a given estimate must be lower than the lower limits of the estimate that is compared to. Such cases are significant at $p < 0.05$, though the true (undetermined) p-value will, necessarily, be considerably lower. Variations in community composition were assessed on a set of 10 randomly selected bootstrap-like samples for each geoform type (in each study area), based on β_{BC} calculated from square-root transformed faunal abundance, and then visualised using MDS ordination.

2.3.1.2.2. Seabed nodule cover (fine-scale). Image data were ordered by estimated nodule cover within each study area to investigate variations in faunal characteristics along the nodule cover gradient. Image data were then divided into 5 subsets at nodule-cover breakpoints chosen to yield approximately equal numbers of megafaunal observations in each subset (levels L1 to L5, each representing a different nodule-cover range in each study area). This survey design resulted in 15 subsets (five for each study area) with

markedly larger sizes in the subsets of Area TD, e.g. Area TB and TC subsets were composed of 713 and 675 individuals (respectively) while area TD subsets were composed of 1780 individuals (see Table S3). We applied the same form of bootstrapping as used in the local geomorphological assessment; each image data subset was randomly resampled with replacement until a minimum of 500 individuals were encountered (range: 500–504 ind.), and that process was repeated 1000 times for each nodule-cover level. Again, numerical density (ind. m⁻²), morphotype richness (S_I), and the inverse form of Simpson's index (1/D) were calculated for each bootstrap-like sample while morphotype density (S_A) was calculated following a controlled seabed-area (c. 1000 m²) approach. Mean values and 95% confidence intervals of these parameters were calculated from each bootstrap-like sample set. We report statistical assessments of variations in ecological parameters between study areas by comparisons of the 95% confidence intervals. Variations in community composition were assessed on a set of 5 randomly selected bootstrap-like samples for each nodule-cover level (in each study area), based on β_{BC} calculated from square-root transformed faunal abundance, and then visualised using MDS ordination.

3. Results

3.1. Invertebrate megafauna

3.1.1. Variations in standing stock

Megafaunal density exhibited statistically significant regional variations ($F_{[2,27]} = 3748$, $p < 0.001$, $\eta^2 = 0.996$). Mean faunal density in Area TD (0.44 ind. m⁻²) was about three times higher than in Area TB (0.14 ind. m⁻²) and almost four times higher than in Area TC (0.11 ind. m⁻²; Fig. 4A). Variations in density were statistically significantly different across all study areas (pairwise comparisons, $p < 0.001$). Density of different functional groups was consistently higher in Area TD. For instance, mean density of sessile suspension feeding fauna (predominantly sponges and anemones) was substantially higher in Area TD (0.22 ind. m⁻²) than that in both TB and TC (0.09 and 0.06 ind. m⁻², respectively); in addition, mean density of mobile deposit-feeding fauna (predominantly brittle stars) was > 5 times higher in Area TD (0.17 ind. m⁻²) than in TB and TC (0.03 ind. m⁻², in each area). Mean density of mobile predators & scavenger fauna (predominantly crustaceans) was also substantially higher in Area TD (2.01 ind. 100 m⁻²) than in areas TB (0.70 ind. 100 m⁻²) and TC (0.76 ind. 100 m⁻²).

Locally, faunal density exhibited substantial variations, both between different geoforms and across the nodule-cover gradient mapped in each study area. At the broad scale, substantially and consistently higher faunal densities were found in Hill areas (e.g. higher mean values and non-overlapping confidence intervals) than in Plain and particularly Trough geoforms (Fig. 4B–D). In Area TD these differences were more pronounced and the faunal density found in Troughs was also substantially lower than in Plain areas (Fig. 4D). At a finer scale, faunal density in all study areas was substantially and consistently reduced in the lowest nodule cover level (L1) compared to areas with higher nodule-cover (L2 to L5), where similar mean densities were found (Fig. 5A). This pattern was more pronounced in Area TD, where faunal density increased from 0.36 ind. m⁻² in the lowest nodule cover level (L1, mean nodule-cover: 1.9%) to 0.52–0.56 ind. m⁻² in the rest of areas (L2 to L5, mean nodule-cover > 9.1%).

3.1.2. Variations in alpha-diversity

Patterns in taxon richness (S_I) and taxon density (S_A) varied between study areas. While mean S_I was broadly consistent (Fig. 4E), with mean values ranging 72–76 morphotypes in c. 500 ind. (Fig. 4E), mean S_A (Fig. 4I) was significantly different between study areas ($F_{[2,70]} = 464.9$, $p < 0.001$, $\eta^2 = 0.92$) owing to the inherently different faunal densities in these locations (Fig. 4A). A statistically

significantly higher S_A (pairwise comparisons, $p < 0.001$) was found in Area TD (68.8 morphotypes in c. 1000 m²) compared to areas TB and TC (39.2 and 35.7 morphotypes in c. 1000 m², respectively), which were not significantly different (pairwise comparisons, $p > 0.05$). Taxon accumulation curves supported these results; the larger S_A in Area TD generated a different taxon accumulation pattern in this study area when assessed in relation to seabed surface sampling effort (a significantly higher richness detectable in samples > 1000 m², Fig. 6A), while individual-based sampling assessments revealed a relatively similar taxa accumulation pattern in all three study areas (Fig. 6B). Mean 1/D index (taxa evenness) was significantly different between study areas ($F_{[2,27]} = 82.9$, $p < 0.001$, $\eta^2 = 0.86$), and variations were significant across all sites (pairwise comparisons, $p < 0.001$). The assemblage in Area TC had the highest values of 1/D index (19.9 effective taxa in c. 500 ind.), followed by Area TB (15.1 effective taxa in c. 500 ind.), and Area TD (11.3 effective taxa in c. 500 ind.; Fig. 4Q).

Locally, faunal diversity metrics showed no substantial variations between geoform types (e.g. overlapping confidence intervals, Fig. 4F–H, J–L, N–P), other than slightly lower mean 1/D values in Hill geoforms from areas TC and TD (Fig. 4O and P). S_I was almost invariable across the nodule cover gradient of all study areas (Fig. 5B), but S_A in the lowest nodule-cover level of Area TD (L1, mean nodule cover: 1.9%) was substantially lower than in the most nodule-covered areas (L4–L5, mean nodule-cover > 16.9%; Fig. 5C).

3.1.3. Variations in beta-diversity

From the 256 invertebrate megafauna taxa surveyed in this study, 95 morphotypes were found in all study areas, 57 morphotypes (28 rare; ≤ 3 specimens) were found only in Area TD, 30 morphotypes (25 rare) were found only in Area TB, and 10 morphotypes (8 rare) were found only in Area TC (see Fig. A4A). Area TB and TC shared a higher number of unique taxa (23 morphotypes) than Area TB shared with TD (20 morphotypes) and Area TC did with TD (15 morphotypes). MDS ordination of faunal composition data readily distinguished the samples from the three study areas, particularly those from Area TD from the rest (Fig. 7A). Formal comparison of faunal composition across the assemblages of different study areas indicated a statistically significant difference overall (PERMANOVA, $R = 0.58$, $p = 0.001$) and statistically significant differences in all pairwise comparisons (pairwise PERMANOVA $R \geq 0.69$, $p < 0.007$), although with a smaller dissimilarity exhibited between the assemblages of Area TB and TC (β_{BC} : 43.2%) than each of these with Area TD samples (β_{BC} : 55.0 and 58.9%, respectively).

There were clear variations in the abundance of the most dominant taxonomic groups between study areas (Fig. 8). Mean densities in Area TD were consistently higher across all taxonomic groups except for Holothuroidea, which exhibited a substantially higher density within Area TC than the other areas (Fig. 8H). The higher densities of Alcyonacea (Fig. 8C) and Porifera fauna (Fig. 8D) in Area TD were coupled with an also substantially higher taxonomic richness of these groups in that site. Alcyonacea (Fig. 8C), Bryozoa (Fig. 8E), and Ophiuroidea fauna (Fig. 8G) were almost virtually absent from Area TB and TC compared to TD, while the density of Echinoidea (Fig. 8I) was substantially reduced in Area TC compared to the other areas. The most remarkable variations in distribution at the morphotype level between study areas were: (i) no bamboo corals, e.g. *Bathygorgia* spp. (Fig. 3I) and *Keratoisis* spp., were found in areas TB and TC, while these taxa had a combined total mean density of 0.75 ind. 100 m⁻² in Area TD; (ii) Mean density of the nodule-encrusting sponge *Porifera mtp-5* was substantially reduced in areas TB and TC (0.14 and 0.26 ind. 100 m⁻², respectively) compared to Area TD (2.25 ind. 100 m⁻²). In contrast, mean density of the also nodule-encrusting sponge *Porifera mtp-88* was substantially reduced in Area TD (0.02 ind. 100 m⁻²) compared to areas TB and TC (0.67 and 0.69 ind. 100 m⁻², respectively); (iii) The two most abundant holothurian morphotypes found in Area TC,

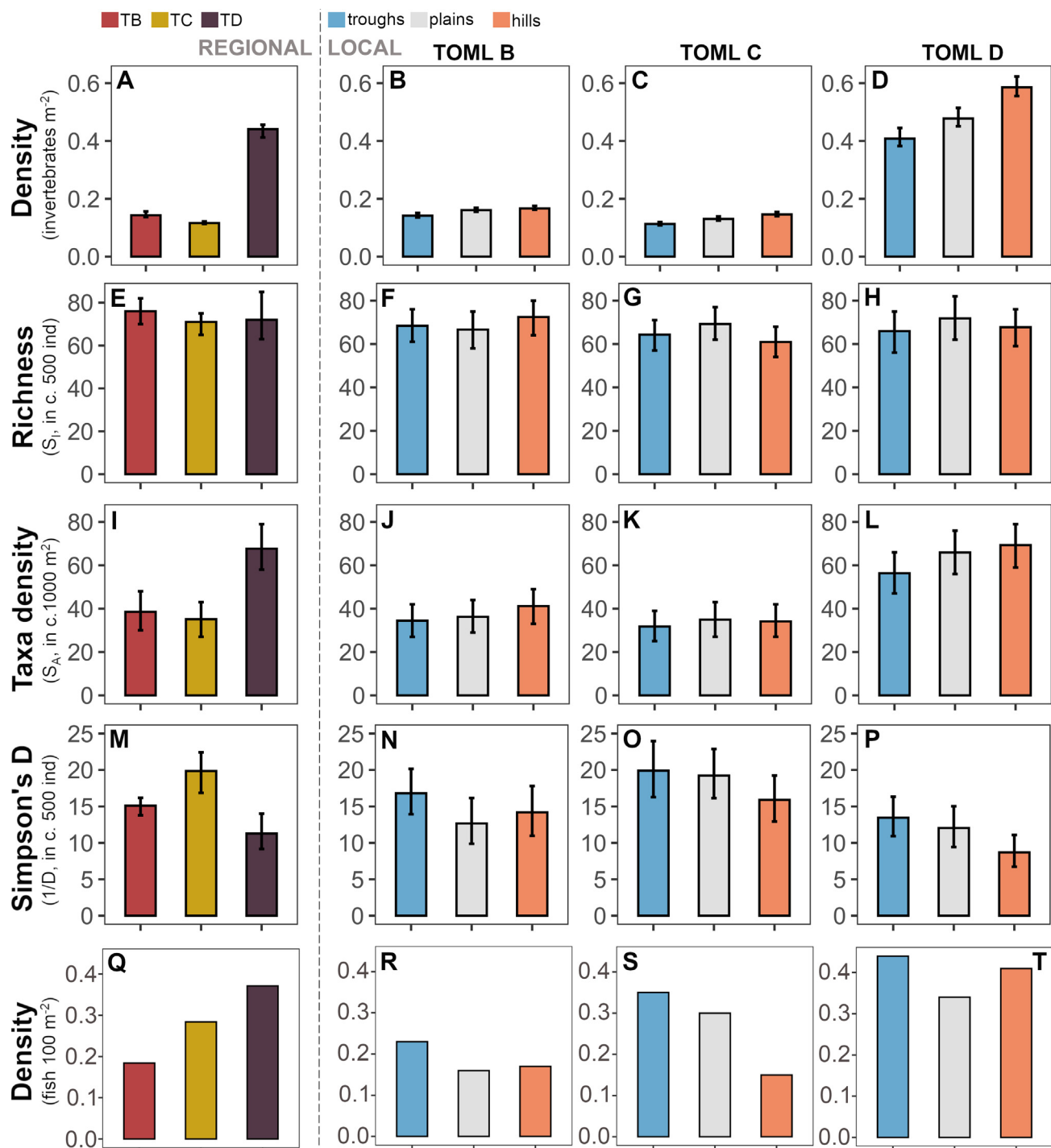


Fig. 4. Regional and local variations in megafaunal density and diversity. Bars indicate mean values across replicate sample sets (regional assessment) or bootstrap-like sample sets (local assessment) surveyed in each study area. Error bars represent 95% confidence intervals. Regional assessment. Study areas: TB, TC, and TD. (A) Invertebrate density. (E) Invertebrate taxa richness. (I) Invertebrate taxa density. (M) Invertebrate heterogeneity diversity; inverse Simpson's index. (Q) Fish density (total). Local assessment. Geoform types: Troughs, Plains, and Hills in respective study areas TB, TC and TD. (B–D) Invertebrate density. (F–H) Invertebrate taxa richness. (J–L) Invertebrate taxa density. (N–P) Invertebrate heterogeneity diversity; inverse Simpson's index. (R–T) Fish density (total).

Amperima sp. mtp-3 and *Ellipinion* sp. mtp-1 (Fig. 3R and S: 0.64 and 1.10 ind. $100 m^{-2}$ in Area TC, respectively), had reduced mean density in Area TB (0.13 and 0.11 ind. $100 m^{-2}$, respectively) and were almost absent from TD (only 2 specimens of *Amperima* sp. mtp-3 found in Area TD); (iv) Mean densities of the ophiuroid *Ophiosphalma glabrum* sp. inc. (Fig. 3V) were two orders of magnitude lower in Areas TB and TC (0.15 and 0.17 ind. $100 m^{-2}$, respectively) compared to that found in Area TD (7.58 ind. $100 m^{-2}$); (v) Mean density of the sea urchin

Aspidodiadema sp. mtp-1 (Fig. 3W) was substantially lower in Area TC (0.19 ind. $100 m^{-2}$) compared to those found in areas TB (1.83 ind. $100 m^{-2}$) and TD (2.13 ind. $100 m^{-2}$).

Locally, we found a markedly higher variability in multivariate assemblage dissimilarity at the finer scale (across the nodule-cover gradient; Fig. 7C) than at the broader-scale (between geoforms; Fig. 7B). At the broader scale, assemblage dissimilarity among different geoforms was consistently higher between Hills and Troughs (Fig. 7B),

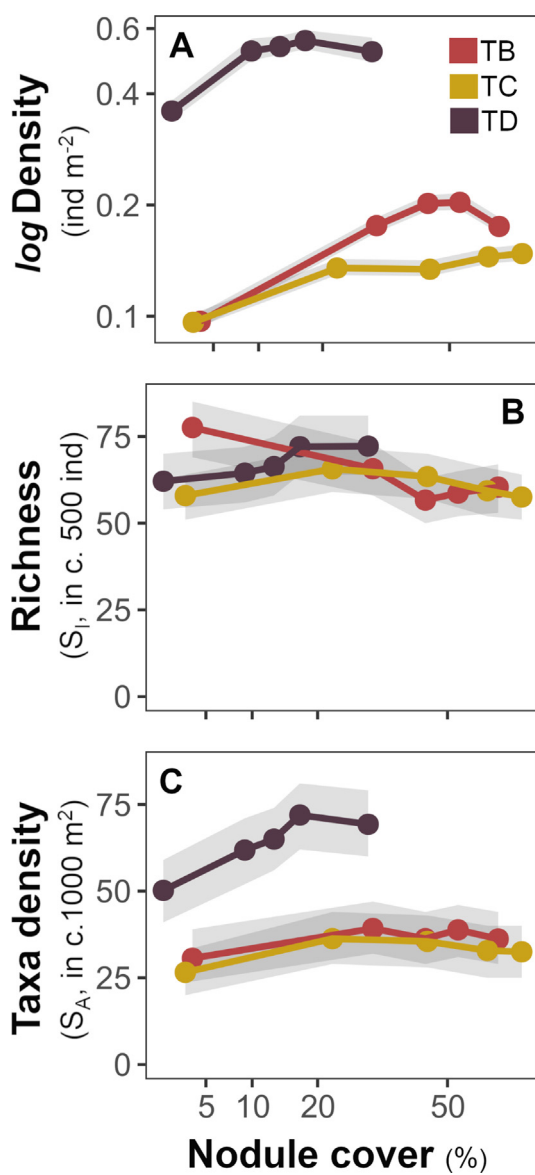


Fig. 5. Local variations in faunal density and diversity across the nodule cover gradient of each study area. Points indicate mean values across bootstrap-like sample sets representing different nodule cover levels surveyed in each study area. Shadowing represent 95% confidence intervals. (A) Invertebrate density. (B) Invertebrate taxa richness. (C) Invertebrate taxa density.

particularly in areas TB and TD (β_{BC} : 40.4 and 41.7%, respectively), while samples from Plains exhibited a higher resemblance with those from the other geoforms (e.g. $\beta_{BC} < 40.0\%$) in all three areas. The most remarkable variations in the abundance of dominant taxonomic groups between geoform types were: i) Sessile Cnidaria (Actiniaria, Alcyonacea, and Antipatharia) consistently exhibited lowest density in Troughs and highest in Hills, in all study areas (e.g. mean densities in Area TD: 11.9 ind. 100 m^{-2} in Troughs; 13.0 ind. 100 m^{-2} in Plains; and 16.1 ind. 100 m^{-2} in Hills), ii) Ophiuroidea density showed the same pattern as sessile Cnidarians (e.g. mean densities in Area TD: 10.6 ind. 100 m^{-2} in Troughs; 15.1 ind. 100 m^{-2} in Plains; and 22.9 ind. 100 m^{-2} in Hills), iii) In contrast to other sessile suspension feeding fauna, Porifera showed no significant variations in density between geoforms (e.g. mean densities in Area TD: 4.8 ind. 100 m^{-2} in Troughs; 5.9 ind. 100 m^{-2} in Plains; and 4.3 ind. 100 m^{-2} in Hills).

At the finer scale, ordination of faunal composition samples (Fig. 7C) readily and consistently distinguished the assemblages of the lowest (L1) and the highest (L5) nodule-cover levels in all study areas

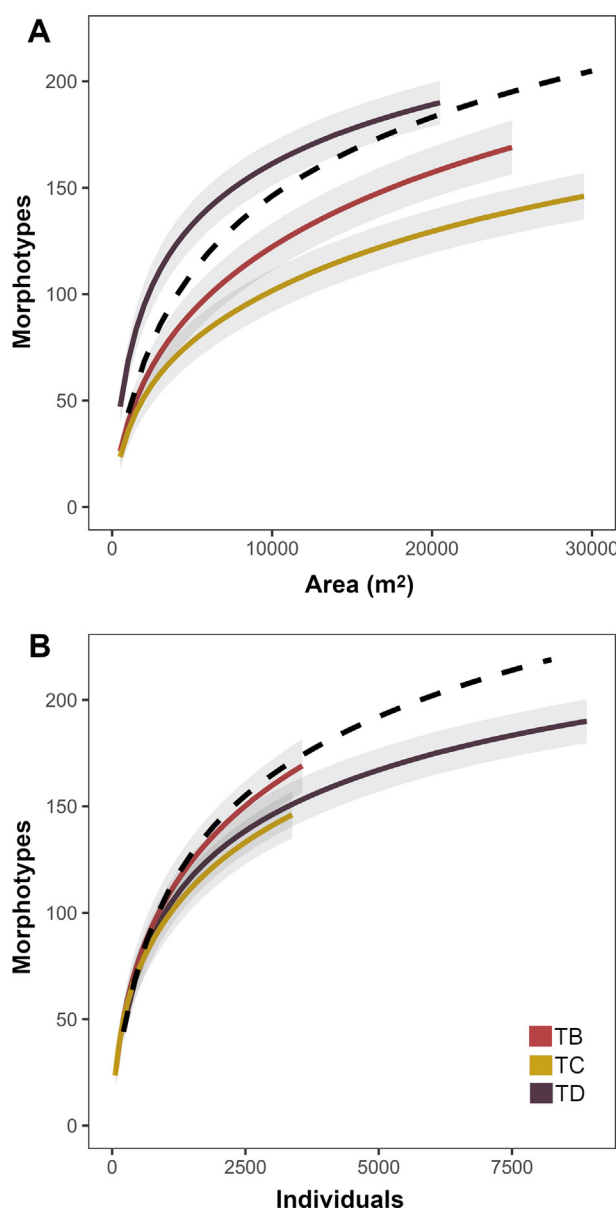


Fig. 6. Invertebrate morphotype accumulation curves for each study area. Dashed line represents combined data. Lines represent mean values across the 100 randomizations performed at each sample unit size increase, for each study area. Shadowing representing 95% confidence intervals. Dashed line represents mean values of curve calculated using whole-study combined data. (A) Curves calculated as a function of the seabed area sampled. Slope coefficients at line end: 0.0022x (TB); 0.0015x (TC); 0.0020x (TD), 0.0007x (Combined). (B) Curves calculated as a function of the number of the individuals sampled. Slope coefficients at line end: 0.0156x (TB); 0.0131x (TC); 0.0046x (TD), 0.0032x (Combined).

(β_{BC} : 47.5, 47.0, and 43.8% in areas TB, TC, and TD respectively). Remarkably, both the assemblages of the lowest and those of the highest nodule-cover levels in areas TB and TC exhibited a higher resemblance with the corresponding ‘homologous’ level (across study areas) than with samples representing other nodule-cover levels surveyed within the same study area. The most notable variations in the abundance of dominant taxonomic groups across nodule-cover gradients were (Fig. 9): i) Actiniaria density increased to an asymptote with increasing nodule cover in all study areas, stabilizing at low (L2) cover levels (Fig. 8A), ii) Ophiuroidea density increased to an asymptote with increasing nodule cover in Area TD (Fig. 9G), iii) Alcyonacea, Antipatharia, and Bryozoa densities increased consistently with

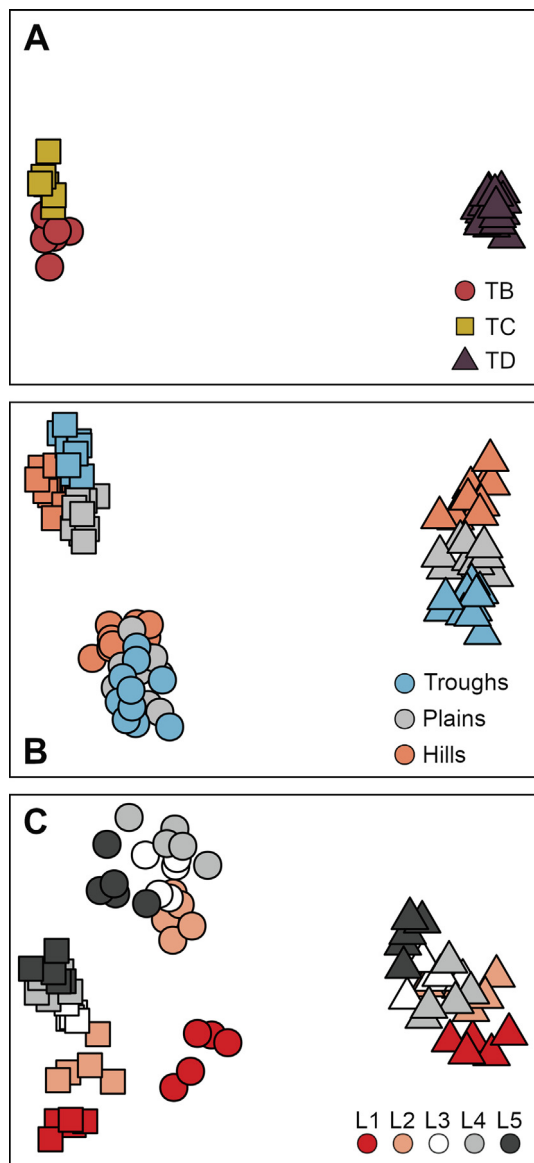


Fig. 7. MDS plots showing regional and local variations in invertebrate assemblage composition. (A) Regional assessment based on replicate samples of each study area (MDS stress: 0.009). Study areas, in all panels: TB (circles); TC (squares); and TD (triangles). (B) Local geomorphological assessment based on 10 randomly selected bootstrap-like samples for each geoform type in each study area (MDS stress: 0.070). (C) Local nodule-cover assessment, based on 5 randomly selected bootstrap-like samples from each of the 5 nodule cover levels (L1: lowest coverage, to L5: maximum coverage) for each study area (MDS stress: 0.011).

increasing nodule cover in Area TD but showed no variations across the cover gradient in the other two areas, where their presence was overall much reduced (Fig. 9B, C and E, iv) Porifera density slightly increased with nodule cover in areas TB and TC (where most of the sponges encountered were nodule-encrusting), but showed no variations across the nodule cover gradient in Area TD, and v) Echinoidea density increased in Area TB, peaking at intermediate cover levels (L3) before reducing at higher nodule cover (unimodal), but showed no variations across the cover gradient in areas TC and TD (Fig. 9I).

3.2. Fish megafauna

Across all three study areas fishes were seen in 0.99% of images (0.66%, 1.02%, and 1.35% in areas TB, TC, and TD respectively).

Overall estimated fish density was 0.38 ind. 100 m^{-2} (3800 fish per km^2). These fishes were classified into 18 distinct morphotypes (see Table S5). The most abundant fish taxon both across the entire image dataset and in every study region was *Ipnops meadi* sp. inc. (Fig. 3γ), with a total of 94 occurrences and making up between 30 and 52% of the fish abundance depending on study site. Regionally, total fish density varied substantially between study areas with densities being higher in Area TD (0.39 ind. 100 m^{-2}) than in areas TB (0.18 ind. 100 m^{-2}) and TC (0.28 ind. 100 m^{-2}) (Fig. 4Q). Assemblage composition also showed some variation between study areas. Notably the second most common taxon in both Area TB and TC (*Leuciscorus* sp., Fig. 3β) was not seen in Area TD, where *Bathyonus caudalis* sp. inc. was instead the second most abundant taxon. Additionally, *B. caudalis* sp. inc. was only seen once in Area TB and not at all in Area TC. In terms of species overlap, 6 of the 18 morphotypes were found across all three regions, and Area TC had the most unique morphotypes (3) (see Fig. A5). Locally, total fish densities were consistently higher in trough landscapes than in plain and hill areas (Fig. 4R–T). Area TC showed the biggest difference between troughs and hills, whereas Area TD had nearly equivalent fish densities on both troughs and hills. The higher density of fish observed in troughs within Area TC and TD resulted from a higher abundance of *I. meadi* sp. inc. in this geoform, while in Area TB this taxon was more abundant on hills. The higher density of fish observed in troughs within Area TB resulted from slightly higher abundances of *Coryphaenoides* sp. (Fig. 3Z) and *Ophidiidae* mtp-1 in these areas. Assessing patterns of fish distribution at the fine scale, with relation to nodule cover was not directly possible for fishes because of the overall low numbers of observations and the unequal sampling of different nodule covers. Overall, 70% of the sampled area had mid to low nodule density (nodule cover 20%), and for the area with the most fish observations, Area TD, 81% of the surveyed area had less than 20% nodule cover. Nevertheless, it is interesting to note that 56% of the *I. meadi* sp. inc. seen were recorded in images with no nodules (0% nodule cover), and all individuals observed were seen in low nodule areas. Excluding *I. meadi* sp. inc., 50% of fish were observed in low nodule areas.

4. Discussion

4.1. Invertebrate megafauna

4.1.1. Regional variations

Clear differences in invertebrate abundance were observed between the three study areas surveyed (Fig. 4A). Density in Area TD (0.44 ind. m^{-2}) was three and four times higher than in areas TB and TC, respectively. Variations of such magnitude in the abyss have typically been linked with differences in the food supply to the benthos, worldwide (Johnson et al., 2007; Rex et al., 2006; Smith et al. 2008) and at the CCZ in particular (Brown et al., 2001; Mullineaux, 1987; Wilson, 2017). For instance, Vanreusel et al. (2016) and Cuvelier et al. (2020) suggested that the higher productivity of the GSR and BGR areas compared to the more northerly APEI3 in the eastern CCZ (e.g. Volz et al., 2018; Fig. 1A) may drive the much higher (i.e. 5 fold) faunal density that these studies found in the southern sites. However, differences in productivity between the three areas surveyed in this study are thought to be minor (1.53–1.58 g C $\text{m}^{-2} \text{ y}^{-1}$, Lutz et al., 2007; Table 1). If water depth is considered as a proxy for food supply, the larger faunal density in the ~500 m shallower Area TD could be explained. However, a significantly reduced density was observed in Area TC compared to TB, which are both at similar depths.

There were clear differences in the predominant nodule size and abundance in each of the three study areas. Nodules were larger and generally less abundant in Area TD than in the other areas. Area TD had the lowest mean surface cover but largest nodule weight per seabed area of all study areas (NM, 2016; Table 1). As variations in nodule size and cover appear to influence megafauna density and distribution

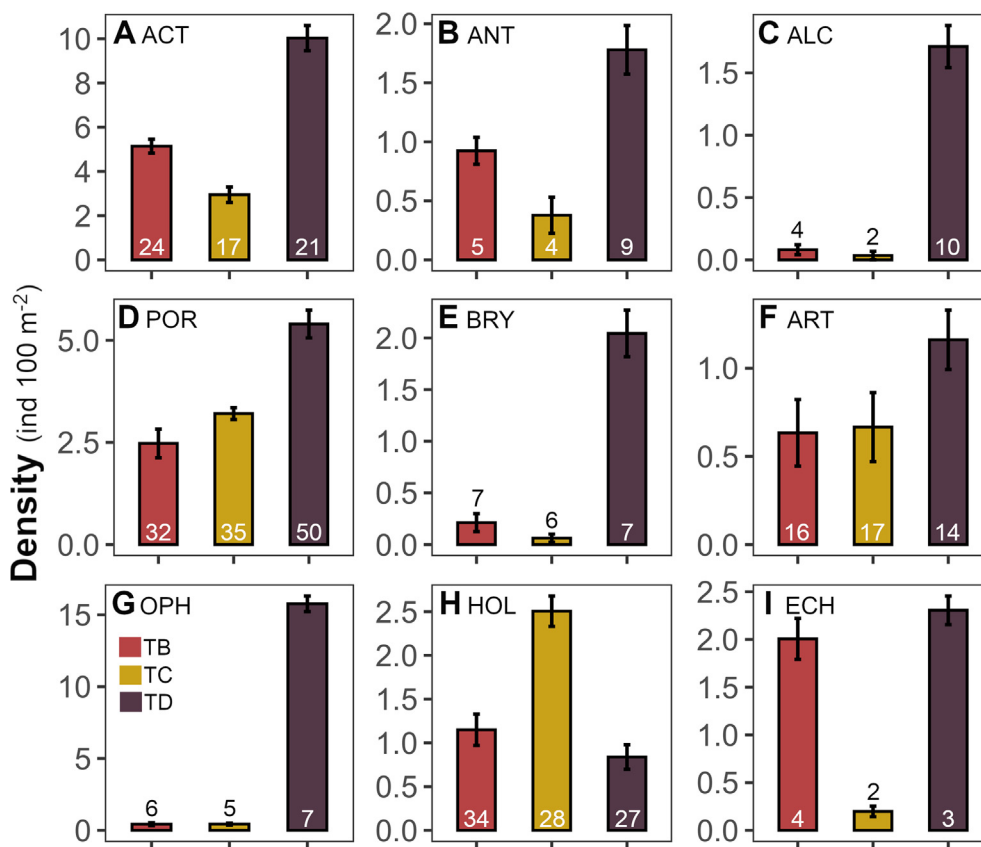


Fig. 8. Regional variations in density and richness of the most abundant faunal groups. Bars indicate mean values across replicate sample sets surveyed in each study area. Error bars represent 95% confidence intervals. Numbers in bars indicate the number of morphotypes encountered in each group. (A) Actiniaria. (B) Antipatharia. (C) Alcyonacea. (D) Porifera. (E) Bryozoa. (F) Arthropoda. (G) Ophiuroidea. (H) Holothuroidea. (I) Echinoidea.

locally (Simon-Lledó et al., 2019b; this study), it is likely that variations in the predominant nodule typology (e.g. shape, volume) may also play an important role in the structuring of communities at the more regional scale. However, it remains unclear how and to what extent these factors regulate the patchy distributions of invertebrate density that seem to characterise the north eastern CCZ region, particularly given the little we know about life history traits of CCZ megafauna.

The three study areas exhibited significantly different assemblage compositions, generally aligning with previous descriptions of communities nearby in the CCZ, and beta-diversity was somewhat proportional to the geographic distance between locations (Figs. 1 and 7A). Variations in composition reflected a substantial degree of taxonomic turnover, perceivable even at Phylum to Class hierarchical levels (Fig. 8). Shifts in the spatial distributions of dominant taxonomic groups were consistent with previous megafaunal assessments conducted in nearby locations (e.g. Amon et al., 2016; Kamenskaya et al., 2013; Simon-Lledó et al., 2019b; Stoyanova, 2012; Vanreusel et al., 2016). For instance, the assemblages of the two western-most study areas (and also most proximal locations), areas TB and TC, had lower densities of Alcyonacea corals and Ophiuroidea, as was reported at the south-east Ifremer area (Vanreusel et al., 2016) which is located right in between the two study areas. The most abundant group in Area TB were Actiniaria, followed by Echinoidea of the genus *Plesiadiadema* sp., as was found in the adjacent Yuzhmorgeologiya area (Kamenskaya et al., 2013). Further north, Area TC exhibited a surprisingly high density of Holothuroidea, the highest reported to date at the CCZ (i.e. 2.5 ind. 100 m⁻²), dominated by a small (max. diameter: ~8 cm) morphotype of the genus *Ellipinion* sp. (Fig. 3S), which accounted for almost half of all the holothurians encountered in Area TC. In contrast, Ophiuroidea were the most abundant group in Area TD, with *Ophistophalma glabrum* sp. inc. dominating the megafaunal assemblage (e.g. 17% of the total invertebrate abundance), exactly as was reported in the UK-1 area (Amon et al., 2016), at a similar latitude. The dominance of *O. glabrum* sp. inc. in Area TD was such that it reduced the taxa evenness in this

area (e.g. Simpson's D; Fig. 4Q). Ophiuroidea abundances appear to gradually increase towards the mid-eastern most sector of the CCZ, where the diversity of this group has also been shown to peak (Christodoulou et al., 2020). Although substantial efforts are still required to further synthesise (and collect) megafaunal distribution data, the observed shifts in the dominant taxonomic groups across sites could be indicative of an underappreciated heterogeneity across the eastern CCZ, and by extension across the whole CCZ area.

Taxon accumulation patterns (Fig. 6) suggest that the differences in the total number of taxa encountered between study areas (TB: 168 mtps; TC: 145 mtps; TD: 189 mtps) reflected the different faunal densities inherent to each location (i.e. S_A, Fig. 4I) rather than actual variations in taxa richness (e.g. S_I, Fig. 4E). Morphotype accumulation curves suggest that the sampling conducted characterized most of the megafaunal assemblage in Area TD and illustrate the large level of sampling effort required (e.g. > 3000 megafaunal specimens) to obtain statistically robust estimations of local taxa richness in abyssal nodule-field areas based on seabed imagery (Ardron et al., 2019; Simon-Lledó et al., 2019a). Morphotype accumulation patterns indicate that further sampling may be required in areas TB and TC (Fig. 6B) to more fully document megafaunal biodiversity, as required in environmental management plans for contractor areas at the CCZ (ISA, 2014). Richness data obtained in Area TD allows a preliminary comparison with the APEI6, the protected area in closest proximity to TOML D, and one of the few CCZ studied areas where the megafaunal sampling effort conducted was also sufficient to adequately quantify this parameter (Simon-Lledó et al., 2019a). There was a larger total taxon richness in Area TD than at the APEI6; excluding fish taxa, a total of 126 invertebrate morphotypes (in 18,500 m²) were found at the APEI6 (Simon-Lledó et al., 2019b), whereas 189 morphotypes (in 20,200 m²) were encountered in Area TD (i.e. mean S_I in c. 500 specimens: 57 in APEI6; 72 in Area TD). There was also a lower megafaunal richness in APEI3 (both in seamount and nodule field areas) than the more southern GSR and BGR sites (Cuvelier et al., 2020). Combined, these

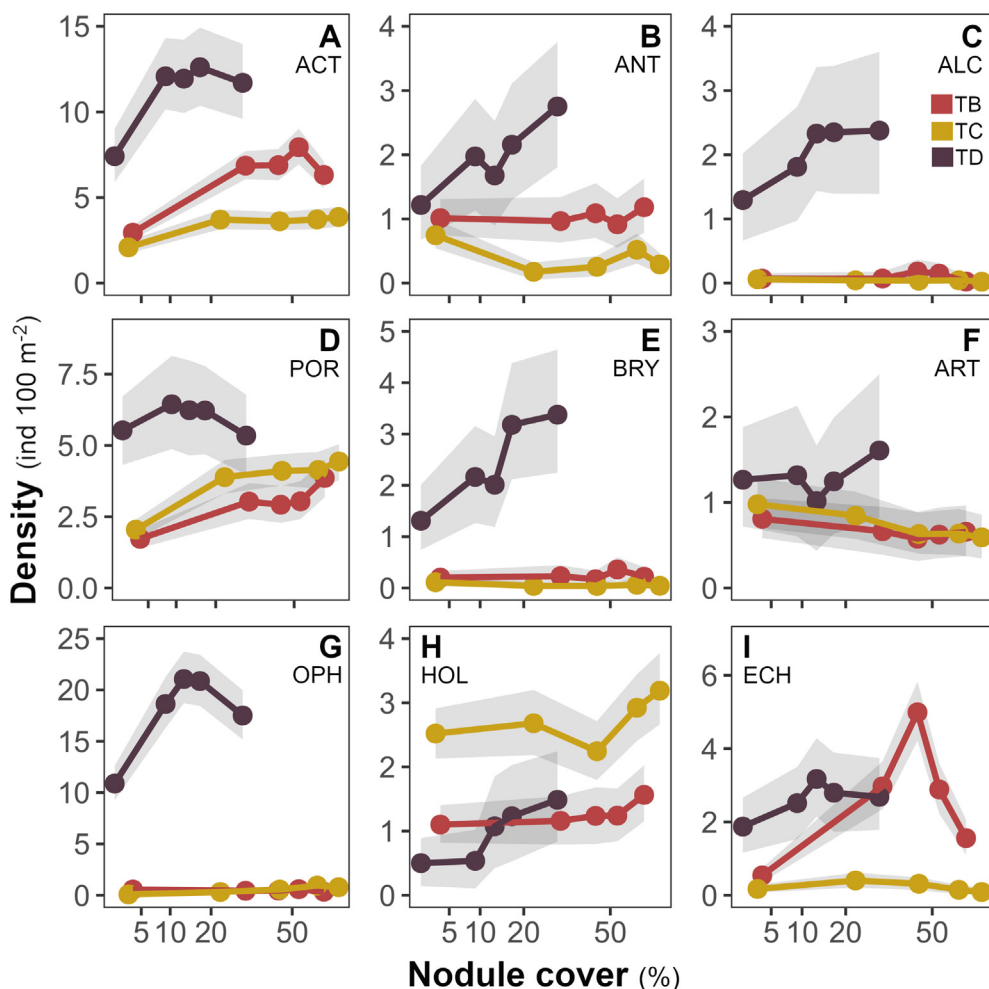


Fig. 9. Local variations in faunal density of the most abundant faunal groups across the nodule cover gradient of each study area. Points indicate mean values across bootstrap-like sample sets representing different nodule cover levels surveyed in each study area. Shadowing represent 95% confidence intervals. (A) Actiniaria. (B) Antipatharia. (C) Alcyonacea. (D) Porifera. (E) Bryozoa. (F) Arthropoda. (G) Ophiuroidea. (H) Holothuroidea. (I) Echinoidea.

results suggest the existence of a latitudinal decrease in megafaunal richness from North to South in this sector of the CCZ, in accordance with the trends described for some macro- and meiofaunal groups (Błażewicz et al., 2019; Bonifácio et al., 2020; Macheriotou et al., 2020; Wilson, 2017). As these and other studies have point out (e.g. Taboada et al., 2018), accumulating evidence is raising concerns on the appropriateness of the north easternmost APEIs (e.g. APEIs 3 and 6) to meet their objective of preserving the full biodiversity range found within this region of the CCZ. Research in the least known south easternmost APEIs (APEIs 8 and 9), and in other almost unexplored contractor areas, is required to further contextualise latitudinal variations.

4.1.2. Local variations

Standing stocks were consistently lowest in Troughs when explored at a broad scale (i.e. tens of km) and in the least nodule-covered areas (L1) when assessed at a fine scale (i.e. tens of meters). The variations across the nodule gradient were much more prominent than between geoforms, as was previously documented in homologous assessments conducted at the APEI6 (Simon-Lledó et al., 2019a, 2019b). In those studies, the abundance of suspension feeders (Actiniaria, Antipatharia, Alcyonacea and Bryozoa) was generally lower in Troughs and higher in Hills, except for Porifera fauna, as we found here. Similarly, reduced densities of Ophiuroidea fauna in nodule-free areas and enhanced densities in Hill areas were also documented at the APEI6. Interestingly, variations in Ophiuroidea density (in Area TD, since virtually absent elsewhere) did not align with those of other deposit feeding fauna, such

as Holothuroidea or Echinoidea, as was found at the APEI6. These variations may be related with enhanced (food) particle flows potentially resulting from the higher hydrographical complexity of hill areas in the CCZ (van Haren, 2018). On the other hand, Ophiuroidea may benefit from micro-scale accumulations of food particles near the base of nodules (e.g. Mullineaux, 1989). In turn, CCZ sessile Cnidarians and Bryozoan taxa typically exhibit a high affinity for nodules (Amon et al., 2016; Simon-Lledó et al., 2019a). Nodules provide stable anchoring for suspension feeders and enable the placement of food-trapping structures into higher, accelerated boundary flows (Mullineaux, 1989), enhancing the abundance of these taxa in areas where nodules are present (Amon et al., 2016; Simon-Lledó et al., 2019b; Vanreusel et al., 2016). Our results concur with Simon-Lledó et al. (2019b) in that a nonlinear, asymptotic relationship exists between standing stock and nodule cover and this response may be explained by resource limitation (Tilman, 1982), i.e. hard substratum is initially limiting, but food resource becomes limiting as attached suspension feeder density increases.

Variations in assemblage composition were more prominent across nodule gradients (β_{BC} range: 43.8–47.5%) than between geoform types (β_{BC} range: 31.1–41.7%), despite the much smaller spatial scale of influence of nodule cover variations. Differences in composition at the local scale reflected the variations in density of the most dominant taxonomic groups, i.e. more prominent across nodule gradients. Surprisingly, although smaller in range, beta-diversity rates associated with local variations in nodule cover appear to be of comparable magnitude to the rates observed at a regional scale (β_{BC} range:

43.2–58.9%) (Fig. 7C). These results stress the key role that nodules appear to play in the structuring of invertebrate communities at the local scale across the CCZ, but also that further research may be needed to understand if/how regional variations in nodule abundance (e.g. Morgan, 2012), or even typology (e.g. Table 1), may also influence megafaunal distributions at more regional scales.

4.2. Fish megafauna

Regional differences in the fish community were evident and followed the patterns observed for invertebrate megafauna though the environmental drivers responsible are not clear. As with invertebrates, a much higher fish density was found in Area TD and density variations did not appear to match with variations in food supply, which are thought to vary little between the study areas. Rather there was a clear decrease in density moving from east to west, as depth increases. Fish density detected in Area TD ($3800 \text{ fishes km}^{-2}$) was similar to those at the APEI6 ($3980 \text{ fishes km}^{-2}$), and at the DISCOL site in the Peru Basin ($3020 \text{ fishes km}^{-2}$), but much higher than reported from the Porcupine Abyssal Plain (751 fish km^{-2}) using generally similar vertical imaging survey methodologies (Drazen et al., 2019; Milligan et al., 2016; Simon-Lledó et al., 2019b, 2019c). In contrast, fish densities detected in areas TC ($2840 \text{ fishes km}^{-2}$) and particularly TB ($1840 \text{ fishes km}^{-2}$) were lower. From a variety of CCZ image databases, *Ipnops meadi* sp. inc. is by far the most frequently seen fish and while this most likely does reflect a true density, it should also be noted that these fishes are especially easy to identify even in high altitude images owing to their large, reflective, dorsally oriented eyes, and they generally remain motionless on the seafloor, showing little to no avoidance behaviour even when approached by large, bright, and noisy remotely operated vehicles (Simon-Lledó, pers comm).

Given their mobility it was somewhat surprising that the fish community composition varied regionally. For instance, a taxon so frequently observed in areas TB and TC (*Leucicorus* sp.) was entirely absent in the images from Area TD. The second most frequently observed taxon in Area TD (*B. caudalis* sp. inc.) was almost entirely absent from the other two sites. Area TD is the furthest east of the three study sites, and Leitner et al. (2017) also documented a significant change in bait-at-tending faunal composition from east to west across the CCZ. It should also be noted that both areas TD and TB are found at lower latitudes and slightly higher presumed nutrient flux than Area TC; however, areas TD and TB were not the most similar regions, nor did they share the largest number of taxa. In fact, only one morphotype was uniquely shared between the two sites while 3 taxa were uniquely shared by areas TD and TC. So, while some studies suggest relationships between abyssal fish community composition and density with food availability (e.g. Armstrong et al., 1992; Linley et al., 2017), a longitudinal driver may be more important in the CCZ.

At the local scale, the higher density of fishes found in Troughs was surprising, given that invertebrate megafaunal densities in this and other studies showed the opposite relationship (Durden et al., 2015; Simon-Lledó et al., 2019a). Further, using baited camera techniques across a bathymetric gradient, abyssal hills (isolated, circular hills) had higher fish relative densities than areas off the hills (Leitner et al., 2017). However, the invertebrate taxa observed in higher abundance on the Hills in this study were sessile Cnidaria and these taxa are not frequently consumed by fishes (Drazen and Sutton, 2017). In the present analysis, higher fish densities in Troughs appears driven by *I. meadi*, which is a benthic fish not seen in baited studies. It is usually found on flat, fine, soft terrain. Indeed, the relationship for areas TC and TD was directly related to the high abundance of this taxon in Troughs, though this did not hold true for Area TB or the APEI6 (e.g. more abundant in hill and plain geoforms; Simon-Lledó et al., 2019a). Given the low abundances of fishes in this study further insights into local scale fish dynamics will require synthesis of data from across the CCZ.

5. Conclusions

This paper presents an assessment of megabenthic faunal distribution in response to multiple environmental factors known to generate habitat variability in abyssal environments. We found significant variations in faunal density and assemblage compositions both at a regional and at a local scale. In agreement with previous studies in the region, broad-scale geomorphological variations (extending tens of km, e.g. Leitner et al., 2017; Simon-Lledó et al., 2019a) and particularly fine-scale variations in polymetallic nodule cover (extending tens of meters; e.g. Simon-Lledó et al., 2019b) emerged as strong drivers of megafaunal variation at the local scale. The presence of nodules appeared to enhance the abundance of the most dominant fauna, somewhat irrespectively of functional group (particularly sessile Cnidaria and Ophiozoidea), driving gradual changes in assemblage compositions (largest dissimilarity rates between the least and the most nodule-covered areas), and enhancing thereby local beta-diversity rates. The effect of nodule presence within a contract area (local scale) was comparable in magnitude to the variation observed between contract areas (regional scale). Finally, preliminary biogeographical exploration of megafaunal variation across the eastern CCZ suggests a substantial degree of underappreciated heterogeneity within this sector, reflected in: i) a longitudinal variation of faunal abundance (decrease towards the west), ii) the clear shifts in the dominant taxa between sites (in $< 350 \text{ km}$), and iii) an apparently higher taxa richness in the more southerly areas of the mid-eastern CCZ (e.g. in the TOML D, GSR, BGR, UK-1 belt) than in the north easternmost sector (APEIs 3 and 6). Results of this contribution shall aid the effective implementation of conservation management strategies at the CCZ, both at local and regional operational levels.

Declaration of Competing Interest

The authors declare the following financial interests/personal relationships which may be considered as potential competing interests: AF was employed by company Fathom Pacific. JP, AA, and CP were employed by company Nautilus Minerals. The remaining authors declare that the research was conducted in the absence of any commercial or financial relationships that could be construed as a potential conflict of interest.

Acknowledgements

We would like to thank Nautilus Minerals Inc., for providing the data for scientific study, and the Ministry of Lands, Survey & Natural Resources, and the Ministry of Meteorology, Energy, Information, Disaster Management, Environment, Climate Change & Communications of the Kingdom of Tonga, particularly to Ms Mafileo Masi and Mr Taaniela Kula, for their support of the project. This work was supported by the United Kingdom Government through the Commonwealth Marine Economies Program, which aims to enable safe and sustainable marine economies across Commonwealth Small Island Developing States. DJ also received support from NERC through National Capability funding to NOC as part of the Climate Linked Atlantic Section Science (CLASS) program, grant number NE/R015953/1. The funders had no role in the study data processing and analysis, decision to publish, or preparation of the manuscript. We would also like to thank the scientific party and crew of the Research Vessel *Yuzhmorgeologiya* for their excellent work during marine operations.

Appendix A. Supplementary material

Supplementary data to this article can be found online at <https://doi.org/10.1016/j.pocean.2020.102405>.

References

- Amon, D., Ziegler, A., Drazen, J., Grischenko, A., Leitner, A., Lindsay, D., Voight, J., Wicksten, M., Young, C., Smith, C., 2017. Megafauna of the UKSRL exploration contract area and eastern Clarion-Clipperton Zone in the Pacific Ocean: Annelida, Arthropoda, Bryozoa, Chordata, Ctenophora, Mollusca. *Biodivers. Data J.* 5, e14598.
- Amon, D.J., Ziegler, A.F., Dahlgren, T.G., Glover, A.G., Goineau, A., Gooday, A.J., Wiklund, H., Smith, C.R., 2016. Insights into the abundance and diversity of abyssal megafauna in a polymetallic-nodule region in the eastern Clarion-Clipperton Zone. *Sci. Rep.* 6, 30492.
- Anderson, M.J., 2001. A new method for non-parametric multivariate analysis of variance. *Austral. Ecol.* 26, 32–46.
- Andrew, N., Mapstone, B., 1987. Sampling and the description of spatial pattern in marine ecology. In: Barnes, M. (Ed.), *Oceanography and Marine Biology; Annual Review*, vol. 25. Aberdeen University Press, pp. 39–90.
- Ardron, J.A., Simon-Lledó, E., Jones, D.O.B., Ruhl, H.A., 2019. Detecting the effects of deep-seabed nodule mining: simulations using megafaunal data from the Clarion-Clipperton zone. *Front. Mar. Sci.* 6.
- Armstrong, J.D., Bagley, P.M., Priede, I.G., 1992. Photographic and acoustic tracking observations of the behaviour of the grenadier *Coryphaenoides* (*Nematonorurus*) armatus the eel *Synaphobranchus bathybius*, and other abyssal demersal fish in the North Atlantic Ocean. *Mar. Biol.* 112, 535–544.
- Błażewicz, M., Józwiak, P., Menot, L., Pabis, K., 2019. High species richness and unique composition of the tanaidacean communities associated with five areas in the Pacific polymetallic nodule fields. *Prog. Oceanogr.* 176, 102141.
- Bonifácio, P., Martínez Arbizu, P., Menot, L., 2020. Alpha and beta diversity patterns of polychaete assemblages across the nodule province of the eastern Clarion-Clipperton Fracture Zone (equatorial Pacific). *Biogeosciences* 17, 865–886.
- Brix, S., Osborn, K.J., Kaiser, S., Truskey, S.B., Schnurr, S.M., Brenke, N., Malyutina, M., Martinez, P.M., 2019. Adult life strategy affects distribution patterns in abyssal isopods – implications for conservation in Pacific nodule areas. *Biogeosciences Discuss.* 1–44. <https://doi.org/10.5194/bg-2019-358>. (Submitted for publication).
- Brown, C.J., Lambshead, P.J.D., Smith, C.R., Hawkins, L.E., Farley, R., 2001. Phytodetritus and the abundance and biomass of abyssal nematodes in the central, equatorial Pacific. *Deep Sea Res. Part I* 48, 555–565.
- Christodoulou, M., O'Hara, T., Hugall, A.F., Khodami, S., Rodrigues, C.F., Hilario, A., Vink, A., Martínez Arbizu, P., 2020. Unexpected high abyssal ophiuroid diversity in polymetallic nodule fields of the northeast Pacific Ocean and implications for conservation. *Biogeosciences* 17, 1845–1876.
- Colwell, R., 2013. EstimateS: Statistical estimation of species richness and shared species from samples. Version 9. User's Guide and Application published at: <http://purl.oclc.org/estimates>.
- Chuar, C.H., Tong, S.J.W., Chim, C.K., Wong, H.P.S., Tan, K.S., 2020. Abyssal macrofaunal community structure in the polymetallic nodule exploration area at the easternmost region of the Clarion-Clipperton Fracture Zone, Pacific Ocean. *Deep Sea Research Part I: Oceanographic Research Papers* 161, 103284.
- Colwell, R.K., Chao, A., Gotelli, N.J., Lin, S.Y., Mao, C.X., Chazdon, R.L., Longino, J.T., 2012. Models and estimators linking individual-based and sample-based rarefaction, extrapolation and comparison of assemblages. *J. Plant Ecol.* 5, 3–21.
- Crowley, P.H., 1992. Resampling methods for computation-intensive data analysis in ecology and evolution. *Annu. Rev. Ecol. Syst.* 23, 405–447.
- Cuvier, D., Ribeiro, P.A., Ramalho, S.P., Kersken, D., Martínez Arbizu, P., Colaço, A., 2020. Are seamounts refuge areas for fauna from polymetallic nodule fields? *Biogeosciences* 17, 2657–2680.
- Dahlgren, T.G., Wiklund, H., Rabone, M., Amon, D.J., Ikebe, C., Watling, L., Smith, C.R., Glover, A.G., 2016. Abyssal fauna of the UK-1 polymetallic nodule exploration area, Clarion-Clipperton Zone, central, Pacific Ocean: Cnidaria. *Biodivers. Data J.* e9277.
- Davison, A.C., Hinkley, D.V., 1997. *Bootstrap Methods and their Application*. Cambridge University Press, Cambridge.
- Dobson, A.J., Barnett, A.G., 2008. *An Introduction to Generalized Linear Models*, third ed. Chapman & Hall/CRC Press, Boca Raton, FL.
- Drazen, J.C., Leitner, A.B., Morningstar, S., Marcon, Y., Greinert, J., Purser, A., 2019. Observations of deep-sea fishes and mobile scavengers from the abyssal DISCOL experimental mining area. *Biogeosciences* 16, 3133–3146.
- Drazen, J.C., Sutton, T.T., 2017. Dining in the deep: the feeding ecology of deep-sea fishes. *Annu. Rev. Mar. Sci.* 9, 337–366.
- Durden, J.M., Bett, B.J., Jones, D.O.B., Huvenne, V.A.I., Ruhl, H.A., 2015. Abyssal hills – hidden source of increased habitat heterogeneity, benthic megafaunal biomass and diversity in the deep sea. *Prog. Oceanogr.* 137, 209–218.
- Durden, J.M., Lallier, L.E., Murphy, K., Jaekel, A., Gjerde, K., Jones, D.O.B., 2018. Environmental Impact Assessment process for deep-sea mining in 'the Area'. *Mar. Policy* 87, 194–202.
- ESRI, 2012. ArcGIS Release 10.1. Environmental Systems Research Institute. Redlands, CA.
- Fox, J., Weisberg, S., Adler, D., Bates, D., Baud-Bovy, G., Ellison, S., Firth, D., Friendly, M., Gorjanc, G., Graves, S., 2016. car: An R Companion to Applied Regression. R package version 3.2-0. <https://CRAN.R-project.org/package=car>.
- Freund, R.J., Little, R.C., 1981. SAS for linear models: a guide to the ANOVA and GLM procedures. Sas Institute Cary, North Carolina.
- Glover, A.G., Smith, C.R., Paterson, G.L.J., Wilson, G.D.F., Hawkins, L., Shearer, M., 2002. Polychaete species diversity in the central Pacific abyss: local and regional patterns, and relationships with productivity. *Mar. Ecol. Prog. Ser.* 240, 157–170.
- Gooday, A.J., Holzmann, M., Caulle, C., Goineau, A., Kamenskaya, O., Weber, A.A.T., Pawłowski, J., 2017. Giant protists (xenophyophores, Foraminifera) are exceptionally diverse in parts of the abyssal eastern Pacific licensed for polymetallic nodule exploration. *Biol. Conserv.* 207, 106–116.
- Hasler, M., Hothorn Ludwig, A., 2011. A Dunnett-type procedure for multiple endpoints. *Int. J. Biostat.* 7, 1.
- Hauquier, F., Macheriotou, L., Bezerra, T.N., Egho, G., Martínez Arbizu, P., Vanreusel, A., 2019. Distribution of free-living marine nematodes in the Clarion-Clipperton Zone: implications for future deep-sea mining scenarios. *Biogeosciences* 16, 3475–3489.
- Hein, J.R., Koschinsky, A., Kuhn, T., 2020. Deep-ocean polymetallic nodules as a resource for critical materials. *Nat. Rev. Earth Environ.*
- Hothorn, T., Bretz, F., Westfall, P., Heiberger, R.M., Schuetzenmeister, A., Scheibe, S., Hothorn, M.T., 2017. multcomp: Simultaneous Inference in General Parametric Models. R package version 1.4-8. <https://CRAN.R-project.org/package=multcomp>.
- Hughes, J.A., Gooday, A.J., 2004. Associations between living benthic foraminifera and dead tests of Syringammina fragilissima (Xenophyophorea) in the Darwin Mounds region (NE Atlantic). *Deep Sea Res. Part I* 51, 1741–1758.
- ISA, International Seabed Authority, 2014. Regulations on Prospecting and Exploration for Polymetallic Nodules in the Area, ISBA/6/A/18 (13 July 2000), amended by ISBA/19/A/9; ISBA/19/A/12 (25 July 2013) and ISBA/20/A/9 (24 July 2014) (Nodules Exploration Regulations).
- ISA, International Seabed Authority, 2020. Polymetallic nodule exploration contracts, <https://isa.org.jm/exploration-contracts/polymetallic-nodules> (last accessed: 10/06/20).
- Janssen, A., Kaiser, S., Meissner, K., Brenke, N., Menot, L., Martínez Arbizu, P., 2015. A reverse taxonomic approach to assess macrofaunal distribution patterns in abyssal Pacific polymetallic nodule fields. *PLoS ONE* 10, e0117790.
- Johnson, N.A., Campbell, J.W., Moore, T.S., Rex, M.A., Etter, R.J., McClain, C.R., Dowell, M.D., 2007. The relationship between the standing stock of deep-sea macrobenthos and surface production in the western North Atlantic. *Deep Sea Res. Part I* 54, 1350–1360.
- Jones, D.O.B., Durden, J.M., Murphy, K., Gjerde, K.M., Gebicka, A., Colaço, A., Morato, T., Cuvier, D., Billeter, D.S.M., 2019. Existing environmental management approaches relevant to deep-sea mining. *Mar. Policy* 103, 172–181.
- Jost, L., 2006. Entropy and diversity. *Oikos* 113, 363–375.
- Kamenskaya, O.E., Melnik, V.F., Gooday, A.J., 2013. Giant protists (xenophyophores and komokiaceans) from the Clarion-Clipperton ferromanganese nodule field (eastern Pacific). *Biol. Bull. Rev.* 3, 388–398.
- Kersken, D., Janussen, D., Arbizu, P.M., 2019. Deep-sea glass sponges (Hexactinellida) from polymetallic nodule fields in the Clarion-Clipperton Fracture Zone (CCFZ), northeastern Pacific: Part II—Hexasterophora. *Mar. Biodivers.* 49, 947–987.
- Lambshead, P.J., Brown, C.J., Ferrero, T.J., Hawkins, L.E., Smith, C.R., Mitchell, N.J., 2003. Biodiversity of nematode assemblages from the region of the Clarion-Clipperton Fracture Zone, an area of commercial mining interest. *BMC Ecol.* 3, 1.
- Langenkämper, D., Zurowietz, M., Schoening, T., Nattkemper, T.W., 2017. BIIGLE 2.0 - browsing and annotating large marine image collections. *Front. Mar. Sci.* 4, 10.
- Leitner, A.B., Neuheimer, A.B., Donlon, E., Smith, C.R., Drazen, J.C., 2017. Environmental and bathymetric influences on abyssal bait-attending communities of the Clarion Clipperton Zone. *Deep Sea Res. Part I* 125, 65–80.
- Levine, T.R., Hullett, C.R., 2002. Eta squared, partial eta squared, and misreporting of effect size in communication research. *Human Commun. Res.* 28, 612–625.
- Linley, T.D., Stewart, A.L., McMillan, P.J., Clark, M.R., Gerringer, M.E., Drazen, J.C., Fujii, T., Jamieson, A.J., 2017. Bait attending fishes of the abyssal zone and hadal boundary: Community structure, functional groups and species distribution in the Kermadec, New Hebrides and Mariana trenches. *Deep Sea Res. Part I* 121, 38–53.
- Lodge, M., Johnson, D., Le Gurun, G., Wengler, M., Weaver, P., Gunn, V., 2014. Seabed mining: International Seabed Authority environmental management plan for the Clarion-Clipperton Zone. A partnership approach. *Mar. Policy* 49, 66–72.
- Lüdecke, D., 2018. sjstats: Statistical Functions for Regression Models R package version 0.17.1. <https://CRAN.R-project.org/package=sjstats>.
- Lutz, M.J., Caldeira, K., Dunbar, R.B., Behrenfeld, M.J., 2007. Seasonal rhythms of net primary production and particulate organic carbon flux to depth describe the efficiency of biological pump in the global ocean. *J. Geophys. Res.* 112. <https://doi.org/10.1029/2006JC003706>.
- Macheriotou, L., Rigaux, A., Derycke, S., Vanreusel, A., 2020. Phylogenetic clustering and rarity imply risk of local species extinction in prospective deep-sea mining areas of the Clarion-Clipperton Fracture Zone. *Proc. R. Soc. B: Biol. Sci.* 287, 20192666.
- Magurran, A.E., 2004. *Measuring Biological Diversity*. Blackwell Science Ltd., Blackwell Publishing.
- Manly, B.F., 2007. *Randomization, Bootstrap and Monte Carlo Methods in Biology*. Chapman & Hall/CRC, Boca Raton, FL.
- McIntyre, F.D., Neat, F., Collie, N., Stewart, M., Fernandes, P.G., 2015. Visual surveys can reveal rather different 'pictures' of fish densities: comparison of trawl and video camera surveys in the Rockall Bank, NE Atlantic Ocean. *Deep Sea Res. Part I* 95, 67–74.
- Mewes, K., Mogollón, J.M., Picard, A., Röhleemann, C., Kuhn, T., Nöthen, K., Kasten, S., 2014. Impact of depositional and biogeochemical processes on small scale variations in nodule abundance in the Clarion-Clipperton Fracture Zone. *Deep Sea Res. Part I* 91, 125–141.
- Miljutina, M.A., Miljutin, D.M., Mahatma, R., Galéron, J., 2010. Deep-sea nematode assemblages of the Clarion-Clipperton Nodule Province (Tropical North-Eastern Pacific). *Mar. Biodivers.* 40, 1–15.
- Milligan, R.J., Morris, K.J., Bett, B.J., Durden, J.M., Jones, D.O.B., Robert, K., Ruhl, H.A., Bailey, D.M., 2016. High resolution study of the spatial distributions of abyssal fishes by autonomous underwater vehicle. *Sci. Rep.* 6, 26095.
- Molodtsova, T.N., Opresko, D.M., 2017. Black corals (Anthozoa: Antipatharia) of the Clarion-Clipperton Fracture Zone. *Mar. Biodivers.* 47, 349–365.
- Morgan, C., 2012. A geological model of polymetallic nodule deposits in the Clarion-Clipperton Fracture Zone. ISA Briefing Paper 1, 12.

- Mullineaux, L.S., 1987. Organisms living on manganese nodules and crusts: distribution and abundance at three North Pacific sites. Deep Sea Res. Part A Oceanogr. Res. Papers 34, 165–184.
- Mullineaux, L.S., 1989. Vertical distributions of the epifauna on manganese nodules: implications for settlement and feeding. Limnol. Oceanogr. 34, 1247–1262.
- Murray, J., Renard, A.F., 1891. Manganese deposits from the HMS Challenger stations. Supplement to: Murray, J.; Renard, AF (1891): Deep-sea deposits (based on the specimens collected during the voyage of HMS Challenger in the years 1872 to 1876). Report on the scientific results of the voyage of H.M.S. Challenger during the years 1873–76; John Menzies and Co., Edinburgh, United Kingdom; original link <http://www.vliz.be/nl/open-marien-archief?module=ref&refid=41584>, 688 pp (pdf 252 Mb), hdl:10013/epic.45942.d002: PANGAEA.
- Oksanen, J., Guillot, Nzuuma Blanchet, F., Friendly, M., Kindt, R., Legendre, P., McGlinn, D., Minchin, P.R., O'Hara, R.B., Simpson, G.L., Solymos, P., Stevens, M.H.H., Szoecs, E., Wagner, H., 2018. vegan: Community Ecology Package. R package version 2.4-6. <https://CRAN.R-project.org/package=vegan>.
- NM, Nautilus Minerals, NA, 2016. NI 43-101 Technical Report. TOML Clarion Clipperton Zone Project, Pacific Ocean. AMC Consultants, Brisbane, QLD, pp. 280.
- Olive, J.A., Behn, M.D., Ito, G., Buck, W.R., Escartin, J., Howell, S., 2015. Sensitivity of seafloor bathymetry to climate-driven fluctuations in mid-ocean ridge magma supply. Science 350, 310–313.
- Pennington, J.T., Mahoney, K.L., Kuwahara, V.S., Kolber, D.D., Calienes, R., Chavez, F.P., 2006. Primary production in the eastern tropical Pacific: a review. Prog. Oceanogr. 69, 285–317.
- Peukert, A., Schoening, T., Alevizos, E., Köser, K., Kwasnitschka, T., Greinert, J., 2018. Understanding Mn-nodule distribution and evaluation of related deep-sea mining impacts using AUV-based hydroacoustic and optical data. Biogeosciences 15, 2525–2549.
- R Core Team, 2017. R: A language and environment for statistical computing. R Foundation for Statistical Computing, Vienna, Austria.
- Radziejewska, T., 2014. Characteristics of the Sub-equatorial North-Eastern Pacific Ocean's Abyss, with a Particular Reference to the Clarion-Clipperton Fracture Zone. *Meiobenthos in the Sub-equatorial Pacific Abyss: A Proxy in Anthropogenic Impact Evaluation*. Springer, Berlin, Heidelberg, pp. 13–28.
- Rex, M.A., Etter, R.J., Morris, J.S., Crouse, J., McClain, C.R., Johnson, N.A., Stuart, C.T., Deming, J.W., Thies, R., Avery, R., 2006. Global bathymetric patterns of standing stock and body size in the deep-sea benthos. Mar. Ecol. Progr. Ser. 317, 1–8.
- Rodgers, J.L., 1999. The bootstrap, the Jackknife, and the randomization test: a sampling taxonomy. Multivar. Behav. Res. 34, 441–456.
- Simon-Lledó, E., Bett, B.J., Huvenne, V.A.I., Köser, K., Schoening, T., Greinert, J., Jones, D.O.B., 2019a. Biological effects 26 years after simulated deep-sea mining. Sci. Rep. 9, 8040.
- Simon-Lledó, E., Bett, B.J., Huvenne, V.A.I., Schoening, T., Benoist, N.M.A., Jeffreys, R.M., Durden, J.M., Jones, D.O.B., 2019b. Megafaunal variation in the abyssal landscape of the Clarion Clipperton Zone. Prog. Oceanogr. 170, 119–133.
- Simon-Lledó, E., Bett, B.J., Huvenne, V.A.I., Schoening, T., Benoist, N.M.A., Jones, D.O.B., 2019c. Ecology of a polymetallic nodule occurrence gradient: implications for deep-sea mining. Limnol. Oceanogr. 64, 1883–1894.
- Simon-Lledó, E., Thompson, S., Yool, A., Flynn, A., Pomee, C., Parianos, J., Jones, D.O.B., 2019d. Preliminary observations of the abyssal Megafauna of Kiribati. Front. Mar. Sci. 6.
- Singh, R., Miljutin, D.M., Vanreusel, A., Radziejewska, T., Miljutina, M.M., Tchesunov, A., Bussau, C., Gal'tsova, V., Martinez Arbizu, P., 2016. Nematode communities inhabiting the soft deep-sea sediment in polymetallic nodule fields: do they differ from those in the nodule-free abyssal areas? Mar. Biol. Res. 12, 345–359.
- Skornyakova, N.S., Murdmaa, I.O., 1992. Local variations in distribution and composition of ferrromanganese nodules in the Clarion-Clipperton Nodule Province. Mar. Geol. 103, 381–405.
- Smith, C.R., De Leo, F.C., Bernardino, A.F., Sweetman, A.K., Arbizu, P.M., 2008. Abyssal food limitation, ecosystem structure and climate change. Trends Ecol. Evol. 23, 518–528.
- Stefanoudis, P.V., Bett, B.J., Gooday, A.J., 2016. Abyssal hills: Influence of topography on benthic foraminiferal assemblages. Prog. Oceanogr. 148, 44–55.
- Stoyanova, V., 2012. Megafaunal Diversity Associated with Deep-sea Nodule-bearing Habitats in the Eastern Part of the Clarion-Clipperton Zone, NE Pacific. In: International Multidisciplinary Scientific GeoConference: SGEM: Surveying Geology & mining Ecology Management; Sofia, vol. 1, pp. 645–651.
- Taboada, S., Riesgo, A., Wiklund, H., Paterson, G.L.J., Koutsouveli, V., Santodomingo, N., Dale, A.C., Smith, C.R., Jones, D.O.B., Dahlgren, T.G., Glover, A.G., 2018. Implications of population connectivity studies for the design of marine protected areas in the deep sea: an example of a demosponge from the Clarion-Clipperton Zone. Mol. Ecol. 27, 4657–4679.
- Tilman, D., 1982. Resource competition and community structure. Monogr. Popul. Biol. 17, 1–296.
- van Haren, H., 2018. Abyssal plain hills and internal wave turbulence. Biogeosciences 15, 4387–4403.
- Vanreusel, A., Hilario, A., Ribeiro, P.A., Menot, L., Arbizu, P.M., 2016. Threatened by mining, polymetallic nodules are required to preserve abyssal epifauna. Sci. Rep. 6, 26808.
- Veillette, J., Sarrazin, J., Gooday, A.J., Galérion, J., Caprais, J.-C., Vangriesheim, A., Étoubleau, J., Christian, J.R., Kim Juniper, S., 2007. Ferromanganese nodule fauna in the Tropical North Pacific Ocean: species richness, faunal cover and spatial distribution. Deep Sea Res. Part I 54, 1912–1935.
- Venkatarathnam, K., Biscaye, P.E., 1973. Clay mineralogy and sedimentation in the eastern Indian Ocean. Deep Sea Res. Oceanogr. Abstr. 20, 727–738.
- Volz, J.B., Mogollón, J.M., Geibert, W., Arbizu, P.M., Koschinsky, A., Kasten, S., 2018. Natural spatial variability of depositional conditions, biogeochemical processes and element fluxes in sediments of the eastern Clarion-Clipperton Zone, Pacific Ocean. Deep Sea Res. Part I 140, 159–172.
- Weiss, A., 2001. Topographic position and landforms analysis. Poster Presentation. 21st Annual ESRI Users Conference. San Diego, CA.
- Wilson, G.D.F., 2017. Macrofauna abundance, species diversity and turnover at three sites in the Clipperton-Clarion Fracture Zone. Mar. Biodivers. 47, 323–347.
- Wright, D.J., Pendleton, M., Boulware, J., Walbridge, S., Gerlt, B., Eslinger, D., Sampson, D., Huntley, E., 2012. ArcGIS Benthic Terrain Modeler. Corvallis, Oregon, Oregon State University, Davey Jones Locker Seafloor Mapping/Marine GIS Laboratory and NOAA Coastal Services Center. Available online at <http://esriurl.com/5754>.